HHS Public Access

Genome scale *in vivo* CRISPR screen identifies *RNLS* as a target for beta cell protection in type 1 diabetes

Erica P. Cai[1,†], **Yuki Ishikawa**[2,†], **Wei Zhang**[2,†], **Nayara C. Leite**[3], **Jian Li**[1], **Shurong Hou**[4], **Badr Kiaf**[2], **Jennifer Hollister-Lock**[1], **Nese Kurt Yilmaz**[4], **Celia A. Schiffer**[4], **Douglas A. Melton**[3], **Stephan Kissler**[2,*], **Peng Yi**[1,*]

[1]Section for Islet Cell and Regenerative Biology, Harvard Medical School, Boston, MA 02215, USA.

[2]Section for Immunobiology, Joslin Diabetes Center, Harvard Medical School, Boston, MA 02215, USA.

[3]Department of Stem Cell and Regenerative Biology, Harvard Stem Cell Institute, Harvard University, Cambridge, MA 02138, USA.

[4]Department of Biochemistry and Molecular Pharmacology, University of Massachusetts Medical School Worcester, MA 01605, USA.

Abstract

Type 1 diabetes (T1D) is caused by the autoimmune destruction of pancreatic beta cells. Pluripotent stem cells can now be differentiated into beta cells, raising the prospect of a cell replacement therapy for T1D. However, autoimmunity would rapidly destroy newly transplanted beta cells. Using a genome-scale CRISPR screen in a mouse model for T1D, here we show that deleting *RNLS*, a GWAS candidate gene for T1D, made beta cells resistant to autoimmune killing. Structure-based modeling identified the FDA-approved drug pargyline as a potential RNLS inhibitor. Oral pargyline treatment protected transplanted beta cells in diabetic mice, leading to disease reversal. Further, pargyline could prevent or delay diabetes onset in several mouse models for T1D. Our results identify *RNLS* as a modifier of beta cell vulnerability and as a potential therapeutic target to avert beta cell loss in T1D.

T1D is caused by the immune-mediated killing of insulin-producing beta cells in the pancreas[1]. The loss of beta cells leads to insulin deficiency that can only be treated by multiple daily insulin injections, a treatment T1D patients depend on for survival for the rest of their lives. Several groups have developed effective differentiation protocols to generate insulin-producing beta-like cells from human embryonic or induced pluripotent stem cells[2]. These advances have raised the prospect of replacing lost beta cells in T1D patients using autologous stem cell-derived beta cells, a strategy with the potential to provide an unlimited supply of cells while also circumventing issues of transplant rejection. However, a key hurdle persists. In the absence of immune suppression, recurrent autoimmunity will rapidly destroy transplanted beta cells. Immune therapies that would induce tolerance to beta cells in T1D patients have not yet been successfully translated from animal models into human[1]. The most promising intervention to date is the use of the anti-CD3 antibody teplizumab that was recently shown to delay disease onset in individuals predicted to develop T1D within a few years[3]. However, no intervention exists that can reverse established disease without broad immunosuppression[4]. To overcome this critical issue, we sought to determine if genetic modifications exist that render transplanted beta cells resistant to autoimmune killing. Others have attempted to produce hypoimmunogenic cells by targeting a series of rationally chosen genes related to immune recognition, including antigen-presenting HLA molecules[5,6]. Although this approach was reported to be partially effective, it requires the complete abrogation of immune surveillance that protects against infection and tumor formation. We speculated that mutations may exist that prevent the autoimmune targeting of beta cells without entirely compromising immune surveillance. We leveraged the selective pressure of autoimmunity in a mouse model for T1D to perform an unbiased genome-wide search for modifiers of beta cell survival in autoimmune diabetes.

RESULTS

CRISPR screen for protective mutations identifies the T1D GWAS candidate Rnls

We designed a screening strategy to search for protective gene mutations in beta cells on a genome scale. To allow for efficient genome editing and experimental reproducibility, we employed the NIT-1 beta cell line, originally derived from a non-obese diabetic (NOD) mouse insulinoma[7]. These cells are suitable for autologous transplantation into NOD mice, the most extensively studied animal model for type 1 diabetes[8]. Of importance, NIT-1 cells transplanted into diabetic NOD mice are rapidly destroyed by autoimmunity (Extended Data Fig. 1). We transduced NIT-1 cells with the mouse lentiviral GeCKO A CRISPR library that comprises ~ 60,000 gRNAs targeting a total of approximately 19,050 genes[9]. Use of a low multiplicity of infection (MOI) ensured that most cells would carry only one mutation. We implanted 10^7 mutant NIT-1 cells into immuno-deficient NOD.*scid* mice and injected splenocytes from diabetic NOD mice into transplant recipients to elicit beta cell killing (Fig. 1). Despite almost total beta cell destruction, we retrieved a small population of NIT-1 cells after 8 weeks that survived the onslaught of autoimmunity. We identified targeted genes by sequencing the gRNAs present in surviving beta cells. We detected only 11 unique gRNA sequences, corresponding to 11 target genes, at significant frequencies in NIT-1 cells that survived autoimmune killing (Fig. 1). Notably, one of these genes was *Rnls*, the candidate gene for a region in the human genome associated both with the overall risk of T1D[10] and

with the age of diabetes onset[11] by GWAS. Based on its prior association with human autoimmune diabetes, we prioritized *Rnls* for validation.

Rnls deletion protects beta cells against autoimmune killing

We generated a *Rnls* mutant NIT-1 cell line (*Rnls*[mut]) using the *Rnls* gRNA identified in the screen (Extended Data Fig. 2). NIT-1 cells were also engineered to carry a luciferase reporter for longitudinal non-invasive imaging of beta cells after transplantation (Extended Data Fig. 1). We started validation experiments using an approach similar to the original genome-wide screen. As illustrated in Fig. 2a, *Rnls*[mut] cells and control NIT-1 cells transduced with a non-targeting (NT) gRNA were co-transplanted on opposing flanks of NOD.*scid* mice. Transplant recipients were then injected with splenocytes from diabetic NOD mice. To control for beta cell survival and proliferation in the absence of autoimmunity, we also monitored beta cell transplants in NOD.*scid* mice that did not receive diabetogenic immune cells. Control NIT-1 cells were killed by autoimmunity within one to two weeks after transplantation, as measured by loss of graft luminescence and analysis of grafts explanted from euthanized mice. In contrast, *Rnls*[mut] NIT-1 cells persisted for up to 2 months in the same recipient mice (Fig. 2b–d and Extended Data Fig. 3). Next, we validated the protective capacity of *Rnls* deletion by implanting NIT-1 cells directly into overtly diabetic NOD mice (Fig. 2e). Again, control NIT-1 cells were rapidly eliminated while *Rnls*[mut] cells survived significantly longer in diabetic NOD mice with ongoing autoimmunity (Fig. 2f–h). Of note, DNA sequencing of the *Rnls*[mut] cell line showed that only ~75% of the cells carried mutant *Rnls* alleles, many of which also carried a wild-type copy of the gene (Extended Data Fig. 2), indicating that a partial loss of function may be sufficient for protection.

We next tested if the disruption of *Rnls* would similarly protect primary mouse beta cells. We isolated pancreatic islets from immuno-deficient NOD.*scid* mice that are devoid of autoimmune infiltrates in the pancreas. We transduced dispersed islet cells with lentivirus encoding rat insulin promoter (RIP)-driven Cas9 endonuclease and either the *Rnls*-targeting (*Rnls*[mut]) gRNA or a non-targeting (NT) control gRNA (Fig. 2i). We transplanted gene edited and control islets cells each under one kidney capsule of the same NOD.*scid* mice. Two weeks later, we injected graft recipients with splenocytes from diabetic NOD mice to induce autoimmune beta cell killing. To control for the effects of gene disruption in the absence of autoimmunity, we also followed islet grafts in NOD.*scid* recipients that did not receive splenocytes from diabetic mice. As anticipated, autoimmunity decreased the size and insulin expression in control grafts (Fig. 2j–l). In contrast, *Rnls*[mut] islets survived autoimmunity and maintained insulin expression. These results show that targeting *Rnls* in primary beta cells was protective in a pathophysiologically relevant model of autoimmune diabetes. Of importance, we found that *Rnls* targeting did not affect the ability of islet cells to secrete insulin (Extended Data Fig. 2).

Rnls mutation diminishes immune recognition of beta cells

We proceeded to ask if *Rnls* deficiency had a direct effect on immune recognition. The expression MHC class I and class II molecules on the surface of *Rnls*[mut] NIT-1 cells was comparable to that of control cells (Fig. 3a–d). *Rnls* mutation did not significantly affect the

response of beta cell-reactive (BCD2.5 TCR transgenic[12,13]) CD4^{+} T cells co-cultured with antigen presenting cells and NIT-1 beta cells[14] (Fig. 3e,f). However, *Rnls*[mut] NIT-1 cells elicited a significantly weaker response from polyclonal beta cell-reactive CD8^{+} T cells isolated from diabetic NOD mice (Fig. 3g,h). Because *Rnls* deficiency diminished the response of autoreactive cytotoxic T cells, we asked if *Rnls*[mut] NIT-1 cells would also be protected against T cell allo-reactivity. To test this, we transplanted *Rnls*[mut] and control NIT-1 cells into opposite flanks of MHC-mismatched C57BL/6 mice. Both beta cell grafts were rapidly destroyed by the strong allogenic response of host immune cells (Extended Data Fig. 3), showing that *Rnls* deficiency did not affect allo-rejection. These data suggest that *Rnls*[mut] beta cells are not impervious to immune detection or killing but that they are less prone to stimulating autoreactive CD8^{+} T cells.

Rnls mutation confers ER stress resistance

A growing body of evidence supports a role for ER stress in the demise of beta cells in diabetes. The unfolded protein response (UPR) that is triggered by ER stress has been implicated in beta cell apoptosis in both T1D and type 2 diabetes[15–17]. Significantly, ER stress was proposed to contribute not only directly but also indirectly to beta cell death in T1D owing its ability to increase the presentation of auto- and neoantigens, for example by affecting post-translational modifications[14,18–20] and antigen processing[21]. We speculated that *Rnls* mutation may affect the cellular response to ER stress and thereby diminish the stimulation of diabetogenic CD8^{+} T cells. To test this notion, we challenged NIT-1 cells with the ER stressor thapsigargin (TG). Control cells were highly sensitive to TG treatment, with concentrations greater than 50 nM killing a majority of cells. Remarkably, *Rnls* mutant cells withstood even a 20-fold greater concentration of TG (Fig. 4a). We obtained similar results with the alternative ER stressor tunicamycin (TC) (Fig. 4b). Further, *Rnls* mutation made cells resistant to the apoptotic effect of the inflammatory cytokines IL-1β and IFN-γ implicated in beta cell stress and killing in T1D[15,22] (Fig.4c). Of note, *Rnls*[mut] NIT-1 cells remained sensitive to mitomycin C and streptozotocin that cause ER stress-independent cell death (Extended Data Fig. 4). These data indicate that *Rnls* deficiency does not prevent all forms of cell death and that its protective effect is limited to specific sources of cellular stress, including inflammatory cytokines associated with T1D[15,22]. To ascertain that ER stress resistance was a direct effect of *Rnls* mutation and not caused by an off-target effect of the *Rnls* gRNA, we generated additional cell lines in which *Rnls* exons 2 to 4 or exon 5 were deleted using different sets of gRNAs. These alternative *Rnls* deficient beta cell lines were again protected against ER stress-induced cell death (Extended Data Fig. 4), confirming that ER stress resistance was a direct result of *Rnls* deletion.

Rnls overexpression sensitizes beta cells to ER stress and autoimmunity

To further evaluate the role of *Rnls* in modifying the sensitivity of beta cells to ER stress and autoimmunity, we overexpressed *Rnls* in NIT-1 beta cells using a lentiviral transgene. While *Rnls* overexpression alone only marginally increased sensitivity to TG-induced killing (Extended Data Fig. 4), it significantly accelerated the autoimmune killing of beta cells implanted into diabetic mice (Extended Data Fig. 5). We proceeded to re-introduce *Rnls* into *Rnls*[mut] cells using a transgene that carried a synonymous mutation within the gRNA target site to prevent CRISPR-Cas9 targeting. *Rnls* re-expression restored the sensitivity of *Rnls*[mut]

cells to ER stress (Extended Data Fig. 4) and accelerated their autoimmune killing in diabetic NOD mice (Extended Data Fig. 5). Collectively, the data show that *Rnls* expression modulates the vulnerability of beta cells to ER stress and autoimmunity.

Rnls modifies the cellular response to ER stress

To understand how *Rnls* deficiency increases ER stress resistance, we measured the UPR that mediates the cellular adaptation to ER stress. We found that the activation of critical ER stress sensors IRE1α[23], PERK[24] and ATF6[25] was diminished in *Rnls*[mut] cells following TG treatment (Fig. 4d and Extended Data Fig. 6). Downstream of these UPR triggers, the phosphorylation of eIF2α, protein levels of ATF4 and splicing of XBP1 were markedly reduced (Fig. 4d and 4e, and Extended Data Fig. 6). The expression of *Chop* and *Txnip*, both implicated in ER stress-induced apoptosis[26–28], was also diminished (Fig. 4f and Extended Data Fig. 6). The data suggest that *Rnls* deficiency increased the threshold of ER stress that triggers the UPR. This would explain how *Rnls* mutation inhibits the pro-apoptotic effect of stimuli that cause cellular stress. The protective effect of *Rnls* deletion was not limited to ER stress, because *Rnls*[mut] cells also better withstood oxidative stress compared to control NIT-1 cells (Extended Data Fig. 6). Consistent with this finding, *Rnls* deficiency increased the expression of a key regulator of the oxidative stress response, NRF2[29] (Fig. 4d and Extended Data Fig. 6). We conclude that *Rnls* deficiency increases the ability of beta cells to withstand the cellular stress involved in their destruction during T1D.

The FDA-approved drug pargyline reproduces the effects of Rnls deletion

Rnls is a flavoprotein oxidase whose cellular function has not yet been elucidated[30]. Its proposed substrates are 2- and 6-dihydroNAD(P)[31], isoforms of β-NAD(P)H, though whether these are physiologically relevant is unknown. However, the crystal structure of human RNLS was solved several years ago[32]. The enzyme uses a flavin adenine dinucleotide (FAD) co-factor for catalysis and is structurally related to other flavoprotein oxidases including monoamine oxidases (MAO). The FDA has approved covalent inhibitors targeting FAD bound to monoamine-oxidase B (MAO-B). Based on structure-based molecular modeling, we predicted that the MAO-B inhibitor pargyline[33] would bind to *RNLS* (Fig. 5a). To test this prediction, we measured the thermal stability of human recombinant RNLS in the presence or absence of pargyline (Fig. 5b,c). Pargyline decreased the thermal stability of RNLS in a dose-dependent manner, suggesting a direct interaction between the drug and the enzyme. We proceeded to ask if pargyline would protect beta cells against ER stress in a manner similar to *Rnls* deletion. Significantly, the drug decreased caspase-3 activation and increased the survival of NIT-1 cells following thapsigargin treatment (Fig. 5d). Moreover, the protective effect of pargyline was also evident in primary islet cell cultures subjected to thapsigargin stress (Fig. 5e).

Pargyline is an oral drug and is water soluble, lending itself to treating mice via their drinking water. We opted to evaluate pargyline's efficacy in a stringent beta cell transplantation model. Recently diabetic NOD mice with severe hyperglycemia (blood glucose > 450 mg/dL) were transplanted with NIT-1 beta cells with or without continuous drug feeding (Fig. 5f). Graft survival was again monitored longitudinally by non-invasive bioluminescence imaging (Fig. 5g). Untreated mice remained hyperglycemic and rapidly

lost their beta cell graft (Fig. 5e–h). Remarkably, pargyline treatment allowed transplanted beta cells to survive in diabetic mice, produce insulin and reverse hyperglycemia (Fig. 5e–i and Extended Data Fig. 7). Pancreas histology three weeks after diabetes onset and beta cell transplantation showed that pargyline-treated mice still harbored a significant number of insulin-rich islets (Extended Data Fig. 7). In contrast, the pancreas of untreated diabetic mice was devoid of insulin staining. These observations suggest that pargyline not only protected grafted NIT-1 beta cells but also endogenous beta cells against autoimmunity, recapitulating the protective effect of *Rnls* deletion. Of note, pargyline did not prevent the allo-rejection of NIT-1 cells transplanted into C57BL/6 mice, indicating that the drug is not immunosuppressive (Extended Data Fig. 8). This again replicates the effects of *Rnls* deletion that conferred protection against autoimmunity but not allo-reactivity. Pargyline also did not decrease hyperglycemia in mice rendered diabetic by high-dose streptozotocin treatment, showing that the drug alone has no glucose-lowering effect (Extended Data Fig. 8). Because pargyline appeared to halt the destruction of endogenous beta cells in diabetic mice, we tested the drug's ability to prevent or delay diabetes. We found that pargyline treatment was protective against diabetes induced by several approaches including cyclophosphamide injection, PD-1 blockade[34] and immune cell transplantation (Extended Data Fig.9). The drug prevented beta cell destruction as evidenced by pancreas histology following disease induction (Extended Data Fig. 9). Pargyline also delayed diabetes induced by multi-low-dose streptozotocin[35] in C57BL/6 mice, a distinct model for immune-mediated diabetes (Extended Data Fig.9). These data suggest that pargyline may carry potential as a preventive therapeutic for T1D.

RNLS deletion confers ER stress resistance to human stem cell-derived beta cells

We identified *Rnls* using the NOD mouse model whose relevance to human T1D has repeatedly been questioned[36]. Notably, *RNLS* had already been implicated in human T1D by GWAS[10,11], suggesting that the effects of *Rnls* mutation on beta cell vulnerability may be conserved in human. To test this, we generated clonal *RNLS* knockout (KO) human induced pluripotent stem cells (SC) by CRISPR-Cas9 gene targeting (Extended Data Fig. 10). *RNLS* deficiency did not affect SC differentiation into beta cells following our published protocol[37] (Fig. 6a–c), and also did not impair insulin secretion (Extended Data Fig. 10). Significantly, *RNLS* KO human SC-beta cells were resistant to TG-induced apoptosis (Fig. 6d,e), reproducing the phenotype of *Rnls* mutant mouse beta cells.

Pargyline phenocopies the effect of RNLS deletion in human stem-cell beta cells

We showed that the FDA-approved drug pargyline binds human recombinant RNLS and that it conferred protection to mouse beta cells in the setting of autoimmunity. We extended these findings by testing if pargyline would replicate the protective effects of *RNLS* deletion in human SC-beta cells. We found that pargyline decreased ER stress-induced cell death in both induced pluripotent and embryonic SC-beta cells (Fig. 6f,g) following TG treatment. Collectively, the data indicate that pargyline phenocopies the protective effects of *RNLS* deletion in both mouse and human beta cells.

DISCUSSION

A beta cell replacement therapy for T1D has become a realistic prospect. Advances in SC-beta cell differentiation now allow the manufacture of billions of patient-derived beta cells for transplantation. The critical hurdle to this therapeutic strategy remains the susceptibility of beta cells to autoimmunity that can only be abrogated by use of broad immunosuppression. Here, we have described the first unbiased and genome-wide search for genes whose suppression would protect beta cells against autoimmunity. We identified a small number of mutations that allowed beta cells to survive in a host with autoimmune diabetes. Although we performed this screen in a mouse model, one of the few candidates that emerged from our stringent experimental system was *RNLS*, a gene that had already been associated with human T1D by GWAS. This supportive evidence from human genetic studies led us to extensively validate the protective effects of *RNLS* mutation in both mouse and human cells. Collectively, our data show that *RNLS* is a modifier of beta cell vulnerability in T1D.

First, this finding may explain why genome variants in the *RNLS* locus impact the overall risk[10] and the age of onset[11] of T1D. How disease-associated variants modify *RNLS* function or expression is unknown and lies beyond the scope of the present study. Nevertheless, in light of our results, exploring how this candidate T1D risk gene is regulated seems warranted.

Second, the data underscore the central role of beta cell ER stress in promoting islet autoimmunity. The ER and oxidative stress resistance afforded by *Rnls* deficiency was correlated with protection against autoimmunity, consistent with a growing body of literature that implicates beta cell ER stress in T1D[15]. We propose that *RNLS* may associate with the risk of T1D owing to its role in modulating the stress-resistance of pancreatic beta cells that, in turn, modifies their susceptibility to autoimmune targeting. The detailed mechanism by which *RNLS* impacts on the cellular response to ER and oxidative stress remains obscure. This mechanism will certainly prove challenging to elucidate given that even the biochemical function of *RNLS* is yet to be understood. Notwithstanding, our finding that *RNLS* deficiency renders beta cells resistant to cellular stress provides a likely albeit speculative explanation for their protection from autoimmunity, consistent with the emerging notion that beta cell stress is central to T1D pathogenesis. Of note, *RNLS* may have enzyme-independent properties as an extracellular receptor ligand in other tissues[38,39]. The RNLS protein was reported to be protective in this role[40] that seems to be distinct from the enzymatic function underlying the results presented here.

Significantly, our discovery that *RNLS* deficiency endows beta cells with the ability to resist autoimmunity suggests a genetic engineering solution to beta cell replacement in T1D that would interfere neither with the identity of the beta cell nor with immunity and immune surveillance. We envisage that *RNLS* deletion could be a safe and effective modification in SC-beta cells to overcome autoimmunity in patients with T1D. Because this approach targets beta cells, it may be ideally suited in combination with an immune therapy such as teplizumab that targets T lymphocytes and that was recently shown to delay disease progression[3]. Conceivably, *RNLS* deletion could also be combined with other protective

candidates identified in this screen, once these have been validated, to provide even more robust protection against autoimmunity.

Finally, we have identified an FDA-approved drug that replicates the protective effect of *RNLS* deletion. Its apparent efficacy in protecting beta cells and preventing diabetes onset in mice, together with its favorable safety profile, should make pargyline - and other MAO-inhibitors predicted to target RNLS - worthy of further evaluation for the prevention or treatment of T1D.

In sum, our unbiased screen for therapeutic targets in a mouse model for T1D converged with human GWAS data to identify *RNLS* as a modifier of beta cell vulnerability. Our discovery that an FDA-approved drug can be repurposed to inhibit *RNLS* will facilitate further evaluation of this therapeutic candidate.

METHODS

Mice

Nonobese diabetic (NOD) mice, NOD.scid (NOD.CB 17-*Prkdc^scid*/J) and C57BL/6J were purchased from the Jackson Laboratory (Bar Harbor, ME). Animals were housed in pathogen-free facilities at the Joslin Diabetes Center and all experimental procedures were approved and performed in accordance with institutional guidelines and regulations.

CRISPR GeCKO A library screen

The mouse GeCKO-v2 (Genome-Scale CRISPR Knock-Out) A lentiviral pooled library was obtained from Addgene (Addgene, #1000000052), targeting 19050 with 3 gRNAs/gene[42] and was prepared as previously described[43]. Wild type NIT-1 cells (ATCC #CRL-2055) were infected with GeCKO A CRISPR lentiviral library at MOI=0.3, and then selected by puromycin (2 μg/ml) at day 3 post lentivirus infection. 10^7 mutant NIT-1 cells were transplanted subcutaneously into 8-week-old female NOD.*scid* mice, and 10^7 of diabetic NOD splenocytes in 200 μl sterile PBS were injected intravenously at the same time to induce autoimmunity. NOD.*scid* mice with subcutaneously transplanted mutant NIT-1 cells but without diabetic NOD splenocytes injection were used as control (non-autoimmune group). Diabetic NOD splenocytes were isolated from spontaneously diabetic female NOD mice as described previously[44]. In brief, the spleen was mechanically disaggregated into a single-cell suspension. Red blood cells were lysed using a hypotonic buffer, and cells were washed in PBS and counted prior to injection. We terminated the screen at 8 weeks post-injection and the remaining grafts were retrieved from both the autoimmune group and the non-autoimmune group of mice. Genomic DNA was extracted from the grafts (Quick-gDNA midiprep kit, Zymo Research), the NGS (Next Generation Sequencing) libraries were prepared as previously described[45], and subjected to NGS sequencing analysis (Novogene, CA). The gRNA sequences from the NGS sequencing data were extracted using standard bioinformatics methods, and the distribution of gRNAs were calculated as Count Per Million (CPM).

Cell line

NIT-1 (#CRL-2055) and 293FT (#R7007) cell lines were obtained from ATCC and Thermo Fisher Scientific respectively. Cells were maintained in DMEM (Gibco, 10313039), supplemented with 10% fetal bovine serum (FBS, Gibco), glutagro and penicillin/ streptomycin (Corning), in a 37° C incubator with 5% CO_2. To generate control and $Rnls^{mut}$ NIT-1 cells, non-targeting (NT) gRNA (5' TAAAAACGCTGGCGGCCTAG 3', MGLibA_67395) and $Rnls$ gRNA (5' CTACTCCTCTCGCTATGCTC 3', MGLibA_46009) were cloned into LentiCRISPR-v2 vector, and the NT or $Rnls$ gRNA containing lentivirus was used to establish these cell lines, respectively. $Rnls$ mutation in $Rnls^{mut}$ cells was confirmed by deep sequencing analysis (MGH DNA Core Facility, Cambridge, MA). The $Rnls$ overexpressing NIT-1 cell line was generated by lentiviral infection of wild-type (WT) NIT-1 cells with EF1α promoter-driven full-length mouse $Rnls$ (Of note, the full-length mouse $Rnls$ that we cloned and used is based on the annotation from the NCBI database in late 2017 that included 300aa, the $Rnls$ annotation in NCBI was updated in March 2019 and now encodes a protein with 42 additional amino acids at the N-terminus). For generation of $CiRnls$-expressing $Rnls^{mut}$ cells, $Rnls$ mutant NIT-1 cells were transduced with lentivirus carrying a CRISPR-immune EF1α promoter-driven full-length mouse $Rnls$ ($CiRnls$) carrying a synonymous mutation in the $Rnls$ gRNA target site. The modified gRNA targeting site sequence used in $CiRnls$ was 5' TTATAGTAGCCGGTACGCA 3'. The $Rnls$-deficient NIT-1 cell lines ($Rnls$ Ex2/4 and $Rnls$ Ex5) were generated following previously published protocols[46]. Two gRNAs were designed to target the 5'- and 3'-end of $Rnls$ exon 2–4 or exon 5 genomic DNA sequences. gRNA sequences for exon 2–4 were 5'CGTCTGGGAAGTCTTGGTCG 3' and 5' CGGGACTCATCCCATTGTCG 3'; gRNA sequences for exon 5 were 5'GGGGAGTGAGGATAGGATAG 3' and 5' TCCGTAGTGGTTTTAGAGTG 3'. The lenti-multi-CRISPR plasmid (Addgene, #85402) was used to express two single gRNAs cassettes for the deletion of exons 2–4 or exon 5 of $Rnls$. The two gRNAs cassettes were amplified by Phusion High-Fidelity PCR kit: 40 cycles: 98°C, 15 sec; 60°C, 15 sec; 72°C, 30sec. The PCR products were digested with BbsI (Invitrogen) and sub-cloned into the pSpCas9(BB)-2A-Puro (PX459) v2.0 vector (Addgene, #62988). NIT-1 cells were then transfected with these plasmids by polyethylenimine (Fisher Scientific), followed by puromycin selection. All plasmid sequences were verified by Sanger sequencing before transduction and transfection.

Preparation and transplantation of primary islets

Islets were prepared and purified as described previously[47] from 8-week-old female NOD.*scid* mice. Briefly, the pancreas was perfused with collagenase type V /cold Hank's balanced salt solution (HBSS) and was immediately removed by surgical dissection. The pancreatic tissue was digested at 37°C water bath for 15–17 min. The digested tissue was then washed with cold HBSS for three times, followed by a Histopaque gradient separation. Islets were handpicked under dissection microscope. Purified NOD.*scid* islets were disrupted into to small clusters by gentle pipetting and then cultured in a low-attachment plate in RMPI 1640 medium (Gibco), supplemented with 10% FBS and penicillin/ streptomycin for viral infection and reaggregation. Lentivirus encoding a NT or $Rnls$ gRNA together with Cas9 endonuclease under the control of the rat insulin promoter (RIP) was added to the culture media for overnight infection. The next day, islets were washed with

culture media twice and ~300 islets were transplanted under each kidney capsule of 8-week-old female NOD.*scid* mice. Graft recipients were left to recover from surgery for two weeks, then mice were randomly assigned to non-autoimmune and autoimmune groups. Mice in the autoimmune group were injected intravenously with 10^7 splenocytes purified from spontaneously diabetic female NOD mice. Splenocytes were prepared as described above (see CRISPR GeCKO A library screen section). At day 25 post splenocyte injection, islet grafts were retrieved for gene expression analysis by quantitative real-time PCR (qPCR).

Quantitative real-time PCR (qPCR)

Cells or islet grafts were treated with TRIzol (Thermo Fisher Scientific) for RNA extraction following the manufacturer's protocol. Purified RNA was reverse-transcribed into cDNA using the SuperScript IV first-strand synthesis kit (Invitrogen). *Insulin 1* (Mm01259683_g1), *Glucagon* (Mm01269055_m1) and *Hprt1* (Mm0302475_m1) probes for TaqMan assays were purchased from Thermo Fisher Scientific. Gene expression levels of *Chop* and *Txnip* were analyzed by SYBR green PowerUp qPCR assays (Applied Biosystems). Primer sequences used for *Chop*: forward - 5' CCACCCACACCTGAAAGCAGAA 3'; reverse - 5'AGGTGAAAGGCAGGGACTCA 3'; *Txnip*: forward - 5' TCAAGGGCCCTGGGAACATC 3'; reverse - 5' GACACTGGTGCCATTAAGTCAG 3'. All qPCR assays were performed using a QuantStudio 6 Flex Real-Time PCR system (Applied Biosystems).

Cell viability assay

Cells were seeded in 96-well white plate (50,000 cells / well) for overnight culture with or without thapsigargin, tunicamycin, streptozotocin (Sigma-Aldrich), mitomycin C (Fisher Scientific), murine recombinant IL-1β (BioLegend) and IFN-γ (Peprotech), or hydrogen peroxide (H_2O_2, Fisher Scientific) at the indicated concentrations. Cell viability was assessed after 24 h using the CellTiter-Glo luminescence Cell Viability Assay (Promega).

Islet cell ER stress assay

8-week-old female NOD.*scid* mice were given drinking water with or without pargyline (5 μg/ml) *ad libitum* for 1 week. Islets were prepared and purified as described above. Purified NOD.*scid* islets were cultured in a low-attachment plate in full culture media with or without pargyline (2 μg/ml) with or without 1 μM thapsigargin for 5 h. Islet protein samples were collected as described below (see Western blotting). 20 μg denatured islet proteins were used for SDS-PAGE electrophoresis. Cleaved Caspase-3 (Cell signaling, #9664S) and GAPDH (Cell signaling, #2118) were blotted to detect apoptotic pathway activation.

In vivo bioluminescence imaging

NIT-1 cell lines were engineered to constitutively express the firefly luciferase gene (Luc2) driven by the EF1α promoter *via* lentiviral delivery, except in Fig.S1, where a CMV-Luc2 construct was used. Mice transplanted with luciferase-expressing cells were injected with D-luciferin intraperitoneally at a dose of 150 mg/kg for bioluminescence imaging. D-luciferin (Gold Biotechnology, Cat# LUCK) solution was prepared in sterile DPBS (without calcium

or magnesium) at a concentration of 15 mg/ml and filtered (0.22 μm) prior to injection. Luminescence was measured using an IVIS Spectrum imaging system (PerkinElmer).

Xbp1 splicing assay

Cells were treated either with DMSO or thapsigargin at 1 μM for 5 h. RNA was extracted by TRIzol and reverse transcribed into cDNA as described for qPCR. Spliced (s) and unspliced (u) *Xbp1* cDNA were amplified by PCR using the Phusion High-Fidelity DNA polymerase (Invitrogen) for 35 cycles: 94°C, 10 sec; 64°C, 30 sec; 72°C, 30sec. The PCR products of *Xbp1* were sized at 473bp (*Xbp1u*) and 447bp (*Xbp1s*) and segregated by electrophoresis using a 3% agarose gel. Ratio of *Xbp1s /Xbp1u* was measured by Adobe Photoshop CC 2019. Primer sequences used for *Xbp1* were forward - 5' AAACAGAGTAGCAGCGCAGACTGC 3' and reverse - 5' TCCTTCTGGGTAGACCTCTGGGAG 3'.

Western blotting

Cell lysates were collected on ice in RIPA lysis buffer containing proteinase and phosphatase inhibitors (cOmplete proteinase inhibitor cocktail, Sigma-Aldrich; Pierce phosphatase inhibitor, Thermo Scientific Fisher). Protein concentrations were measured by Pierce BCA protein assay (Thermo Scientific Fisher). 40 μg denatured cell lysate protein were used for SDS-PAGE electrophoresis (4–20% TGX gel, Bio-Rad). The following primary antibodies were used: PERK (Cell signaling, #3192), phospho-PERK (Thr980, Cell signaling, #3179), ATF4 (Cell signaling, #11815), ATF6 (Novus Biologicals, #NBP1–40256SS), eIF2α (Cell signaling, #2103), phosphor-eIF2α (Ser51, Cell signaling, #3597), IRE1α (Cell signaling, #3294), phosphor-IRE1α (Ser724, Novus Biologicals, #NB100–2323SS), Txnip (MBL, K0205–3), cleaved Caspase 3 (Cell signaling, #9664S), NRF2 (Santa Cruz, #SC365949), GAPDH (Cell Signaling, #2118) and actin (ABclonal, #AC004). All images were obtained and quantified using a C-DiGit blot scanner and the Image Studio software (LI-COR Biosciences).

T7 endonuclease I assay

CRISPR/Cas9 editing in *Rnls*[mut] cells was detected by T7 endonuclease I mismatch cleavage assay. Genomic DNA (gDNA) was purified from control and *Rnls*[mut] NIT-1 cells using Quick-gDNA miniprep kit (Zymo Research). The *Rnls* gRNA targeting site was amplified using the Phusion high-fidelity PCR kit (Thermo Fisher Scientific). Primers for *Rnls* gRNA site PCR were: forward 5' TGCTATAGACAGTTGGGACTTGTTT 3'; reverse 5' ATATTGCGTTCTATTATCAATGGAGATGAAGC 3'. The PCR products (~200 ng) were used to form heteroduplexes by denaturing at 95°C for 5 min and then re-annealing the products in a thermocycler using the following protocol: ramp down to 85°C at −2°C/sec; ramp down to 25°C at −0.1°C/sec; hold at 4°C. 10 units T7 endonuclease I was added to the annealed PCR products and the reaction was incubated at 37°C for 15 min. The digestion reaction was stopped by 1 μl 0.5M EDTA and immediately applied to a 1.5% agarose gel to visualize digested and undigested products by electrophoresis.

CD4^{+} T cell stimulation assay

CD25^{−}CD4^{+} T cells were isolated from BDC2.5-TCR transgenic (Tg) NOD mice using a CD25^{+} regulatory T cell isolation kit (Miltenyi, 130–091-041). Purified CD4^{+} T cells were maintained in culture for three weeks prior to being cultured with NIT-1 cells by weekly stimulation with 1 μM BDC2.5 mimotope in the presence of irradiated splenocytes from NOD.*scid* mice and 20 U/mL IL-2 (Peprotech, 212–12-20UG). The day prior to T cell and NIT-1 co-culture, NIT-1 cell lines were incubated with or without 1 μM Thapsigargin for 5 h. NIT-1 cells were washed extensively with complete DMEM after incubation. 5×10^4 NIT-1 cells were then seeded in each well of a 96-well plate in 100 μL culture medium. The next day, 10^5 BDC2.5-Tg CD4^{+} T cells and 5×10^5 NOD.*scid* splenocytes re-suspended in 100μL RPMI medium were added to NIT-1 cultures. Cells were co-cultured in a 37° C incubator with 5% CO_2 for 24 hours. Cells were treated with BD Golgi plug (diluted 1 in 1,000; BD bioscience, #555029) for the last 5 h of culture. After the incubation, cells were collected and stained with the following antibodies, all of which were purchased from BioLegend; BV785 CD3 (clone 17A2, #100231), PE-Cy7 CD4 (clone GK1.5, #100421), PE anti-TNF-α (clone MP6-XT22, #506306), PE rat IgG1 kappa isotype control (clone RTK2071, #400407), APC IFN-γ (clone XMG1.2, #505810), and APC rat IgG1 kappa isotype control (clone RTK2071, #400411). Zombie Violet Fixable Viability Kit (BioLegend, #423114) was used for dead cell staining, and BD Cytofix/Cytoperm Plus (BD bioscience, #554714) was used for intra-cellular cytokine staining, following the manufacturer's instructions. Flow cytometry was performed on a LSR fortessa instrument (BD Biosciences), and data were analyzed using Flow Jo v10.6 (Flow Jo, LLC).

MHC class I and class II expression analyses

5×10^5 NIT-1 cells were stained with the following antibodies, all of which were purchased from BioLegend; APC anti-mouse H-2Kd (clone SF1–1.1, #116620), APC mouse IgG2a kappa isotype control (clone MOPC-173, #400219), PE anti-mouse IA[k] (Aβ[k]) (clone 10–3.6, #109908) which cross-reacts with mouse I-Ag[7], PE mouse IgG2a kappa isotype control (clone MOPC-173, #400213). Flow cytometry was performed as described above.

CD8^{+} T cell ELISPOT assay

5 μg/mL capture antibody (BD NA/LETM Purified Anti-mouse IFN- γ, BD Biosciences, #51–2525KA) was coated on a 96-well ELISPOT plate (Millipore Sigma, #MAIPS4510) overnight at 4° C. The following day, the plate was blocked with 200 μL complete RPMI medium for 2 hours at room temperature. NIT-1 cells were treated with 100U/mL IFN-γ for 72 hours prior to use in the assay, washed and suspended at 10^5 cells / 100 μL in complete DMEM medium. CD8^{+} T cells were isolated and purified from a female diabetic NOD mouse using mouse CD8a^{+} Isolation Kit (Miltenyi, #130–104-075). 10^5 CD8^{+} T cells were re-suspended in 100 μL complete RPMI medium. NIT-1 cells and CD8^{+} T cells were then mixed at a 1:1 ratio in the antibody-coated 96-well plate and co-cultured for 24 hours in a 37° C incubator with 5% CO_2. Cells were discarded and the plate was washed with PBS-0.1% Tween20 washing buffer three times. 2 μg/mL detection antibody (Biotinylated Anti-mouse IFN- γ, BD Biosciences, #51–1818KA) was added to each well and the plate was incubated for 2 hours at room temperature. Plates were washed three times with

washing buffer and HRP-conjugated streptavidin (BD Biosciences, #557630) was added to each well for one hour. After washing four times with washing buffer and three more times with PBS, substrate solution (R&D, #DY999) was added to each well and incubated for 15–30 min. The reaction was stopped by adding deionized water to each well and the plate was further washed with deionized water. Spots were counted and analyzed on the Immunospot S6 Universal-V instrument (Cellular Technology Limited).

Induced pluripotent stem cell cultures and generation of RNLS knockout iPSCs

Human induced pluripotent stem-cell (iPSC) maintenance and differentiation was carried out as previously described[37]. iPSCs from an individual with type 1 diabetes were obtained from stocks maintained by the Melton laboratory. *RNLS* exon 2 was targeted for deletion using a dual-gRNA strategy in undifferentiated iPSCs. Deletion of the targeted region was verified by PCR and sequencing. iPSCs lines were maintained in cluster suspension culture format using mTeSR3D (Stem Cell Technologies, 03950) in 500 ml spinner flasks (Corning, VWR) spinning at 70 rpm at 37 °C, 5% CO_2 and 100% humidity. iPSCs clusters were dissociated to cell clumps using Gentle Cell Dissociation Reagent (Stem Cell Technologies, 07174) and light mechanical disruption, counted and seeded at 0.7×10^6 cells/ml in mTeSR3D + 10 μM Y27632 (DNSK International, DNSK-KI-15–02).

Differentiation flasks were started 72 h after passage, by removing mTeSR3D medium and replacing with the protocol-appropriate medium and growth factor or small molecule supplement[37]. All experiments involving human cells were approved by the Harvard University IRB and ESCRO committees.

Flow cytometry analyses of iPSC-beta cells

Differentiated clusters, sampled from the suspension culture (1–2 ml), were dissociated using TrypLE Express (Gibco; 12604013) at 37 °C, mechanically disrupted to form single cells, fixed and stained as previously described[41].

Apoptosis assay for iPSC- and ES(HUES8)- beta cells

Differentiated clusters were treated for 24 h with thapsigargin (5 μM), dissociated and stained at room temperature for 30 min using a 1:100 dilution of anti-human CD49a PE (BD 559596)[41] and Apopxin green (ab176750). For pargyline treatment, SC-beta cells were pretreated with 5μM pargyline, for 24h and the drug was kept at 5μM during thapsigargin challenge for another 24h.

RNLS structure analyses and drug-binding modeling

hRNLS uses FAD as a co-factor for catalysis. Therefore, to find compounds that could potentially inhibit hRNLS, we searched Protein Data Bank for protein-inhibitor complex structures that had FAD. MAO-B in complex with inhibitors that covalently attached to FAD were identified through the search. Structural alignments and analysis of the hRNLS crystal structure with these complex structures based on FAD suggested that these inhibitors, for instance Pargyline, may inhibit hRNLS as well. The model of full-length hRNLS in complex with Pargyline was built based on the crystal structures of human renalase (PDB: 3QJ4)[48] and MAO-B rasagiline complex (PDB: 2C65)[49]. The model was first optimized using the

Protein Preparation Wizard[50] from Schrodinger at pH 7.0 and energy minimized with gradually reduced restraints (1000, 5, 0 force constant) on backbone and solute heavy atoms. A multi-stage 100 ns molecular dynamics (MD) simulation using Desmond[51] was performed afterwards. The final frame of the MD simulation was used as the final model in Figure 6a.

RNLS thermal shift assay

Human recombinant RNLS protein was generated by GenScript USA Inc., using the *E. Coli* expression vector pET28a-MBP. RNLS protein was obtained from the supernatant of cell lysates, followed by purification *via* Ni Bio-rad column. 2 mM RNLS dissolved in PBS was incubated with pargyline (Sigma-Aldrich, #P8013) at concentrations of 0, 0.1, 1, 10, 25, 50, 100 mM for 20 min at 4 °C before addition of SYPRO Orange dye (Invitrogen, #S6650) for the measurement of thermal denaturation. The thermal shift assay was performed using the QuantStudio 6 Flex Real-Time PCR system (Applied Biosystems) with an initial temperature hold at 25°C for 2 min, followed by a temperature ramp up to 95°C at a rate of 1°C / s, and a final temperature hold at 95°C for 2 min. Results were collected at 0.25 °C increments. The melting temperature (Tm) of RNLS in the presence and absence of pargyline was calculated by the first derivative of the fluorescence emission as a function of temperature (- dF/dT).

Oral pargyline treatment studies

9-week-old female NOD mice were injected intraperitoneally with cyclophosphamide (200 μg/g of body weight, Sigma-Aldrich, #C0768) for diabetes induction. Diabetic NOD mice (blood glucose >450 mg/dL) identified 10–14 days later were randomly assigned to the control group (normal water) or pargyline treatment group (5 μg/ml pargyline hydrochloride in the drinking water, Sigma-Aldrich #P8013). Treatment was started one week prior to beta cell transplantation. NIT-1 beta cells carrying a luciferase reporter were pre-treated with 5 μM pargyline for 24 h before transplantation. 10^7 NIT-1 cells were transplanted subcutaneously into each diabetic NOD mouse. Blood glucose was monitored every 1–2 days, and graft bioluminescence was imaged every 2–3 days. For preventive studies, 10-week-old NOD mice were pre-treated with or without pargyline water for one week (25 μg/ml), then disease was induced with a single injection of either cyclophosphamide (200 μg/g of body weight) or anti-PD-1 blocking antibody (250 μg/mouse BioCell, clone RMP1–14). Alternatively, disease was induced in 10-week-old NOD.*scid* mice by injection of 10^7 splenocytes from overtly diabetic NOD mice, and cell recipients were treated with or without pargyline water (25 μg/ml). Blood glucose was monitored every 2–3 days for all prevention studies. For the streptozotocin (STZ)-induced diabetes mouse study, 8-week-old male C57BL/6J mice were either injected intraperitoneally with a single high-dose of STZ (150 mg/kg) or with with 5 low doses (50 mg/kg/day) on consecutive days. For high-dose STZ, mice were given drinking water with or without pargyline (25 μg/ml) *ad libitum* three days after STZ injection. For multi-low-dose STZ, mice were pre-treated with pargyline for one week (25μg/ml). Blood glucose was monitored every day in the first week, then every 3–4 days in the second week and every week thereafter for experiments that were monitored for longer than 2 weeks.

Glucose-stimulated insulin secretion and insulin ELISA

Primary islets were isolated from 8-week old CD1(ICR) mice (Envigo) and immediately cultured in a 24-well low-attachment plate. Islets were transduced with lentivirus encoding a non-targeting (NT) or *Rnls* gRNA together with rat insulin promoter-driven Cas9 endonuclease. 72 h later, islets were washed twice with 1 ml Krebs Ringer Bicarbonate HEPES (KRB) buffer containing 2.8 mM glucose, followed by 1 hour incubation at 37°C in 2.8 mM glucose KRB buffer. 0.8 ml KRB was taken out, saved for insulin measurement and replaced with 0.8 ml of 20.2 mM glucose KRB buffer for a final glucose concentration of 16.8 mM for another 1 hour incubation at 37°C. The KRB buffer was again sampled for insulin, then islets were incubated with 30 mM KCl along with 16.8 mM glucose for 1 hour at 37°C before the final insulin sampling. Genomic DNA was purified from islets for normalization of insulin levels to DNA content. Insulin levels were assessed by ultra-sensitive mouse insulin ELISA kit (Crystal Chem, #90080).

Immunofluorescence staining

Pancreases were isolated from control and pargyline-treated mice. Pancreatic sections were stained with anti-insulin (DAKO, #A0564), anti-CD3 (Bio-rad, #MCA500), anti-CD4 (Abcam, #ab183685), anti-CD8 (Novus Biologicals, #NBP1–49045), and Foxp3 (R&D systems, #MAB8214). Images of individual islets were taken with a Zeiss LSM710NLO confocal microscope.

Statistical analyses

Statistical analyses were performed by unpaired or paired tests as indicated using the Prism software version 8.0.2. All data are presented as mean ± SEM. $P < 0.05$ was considered statistically significant. Sufficient sample size was estimated without the use of a power calculation. No samples were excluded from the analysis. No randomization was used for animal experiments. Data analysis was not blinded. All data are representative of two or more similar experiments.

Data availability

The data that support the findings of this study are available from the corresponding authors upon reasonable request.
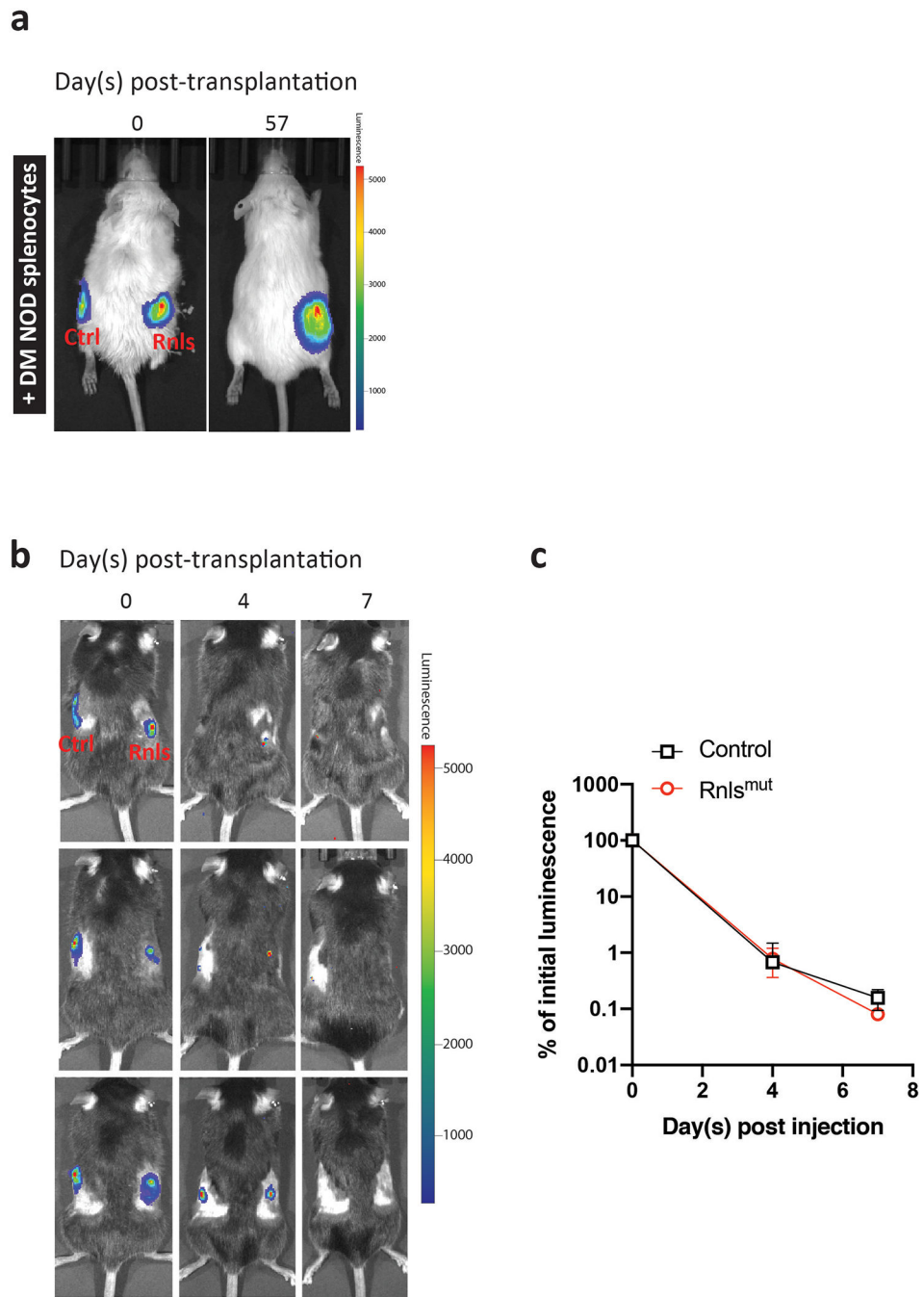
Extended Data

a Day 1 post injection **b** Day 15 post injection
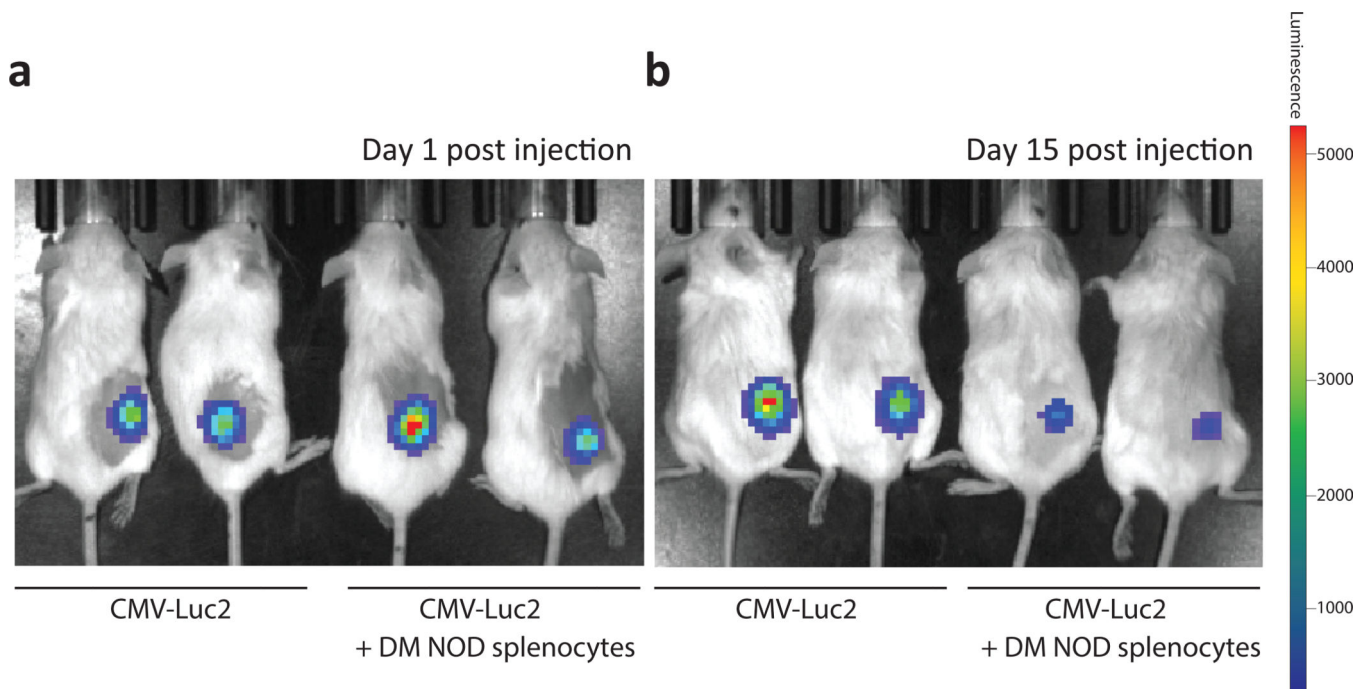
Extended Data Fig. 1. Autoimmune killing of NIT-1 cells in NOD mice can be visualized by bioluminescence imaging.

a,b: Bioluminescence imaging of 10^7 NIT-1 cells transplanted subcutaneously into NOD.*scid* mice. Transplanted cells were engineered to carry a CMV-luciferase2 (Luc2) reporter. Some recipient mice were also injected intravenously with 10^7 splenocytes isolated from spontaneously diabetic (DM) NOD mice to cause beta cell killing. Images were taken at day 1 (**a**) and 15 (**b**) post-injection.
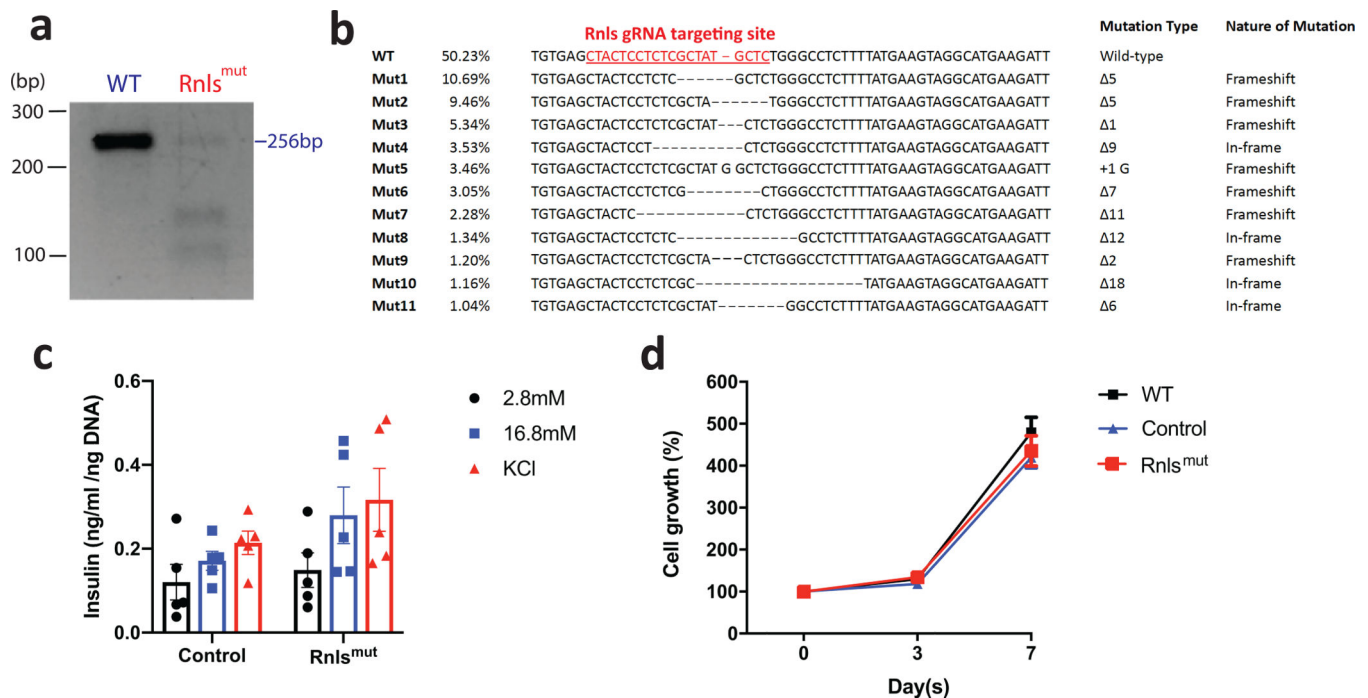
Extended Data Fig. 2. Generation of *Rnls*-mutant beta cells by CRISPR-Cas9 targeting.
a: T7 endonuclease I assay. Genomic DNA from NIT-1 wild-type (WT) and *Rnls*^mut^ cells was tested for CRISPR-Cas9 gene editing events. Cleavage at heteroduplex mismatch sites by T7 endonuclease I digestion was analyzed by agarose gel electrophoresis. DNA from *Rnls*^mut^ cells segregated into multiple digested fragments, indicating efficient mutation of the targeted region in the *Rnls* gene. **b:** Genomic DNA from *Rnls*^mut^ cells was sequenced to identify individual mutations. The *Rnls* gRNA targeting site is labelled in red. The frequency of the wild-type allele and of the most abundant mutations and their predicted consequence (frameshift / in-frame deletion) are shown. These frequencies indicate that 75% of the cells are predicted to carry at least one deleterious mutant allele. **c:** Islets ($\approx$1700) were purified from 8-week old CD1 mice, dispersed and transduced with lentivirus encoding a non-targeting (NT) or *Rnls*-targeting gRNA together with the Cas9 endonuclease driven by the rat insulin promoter. 72 h later, islets were stimulated sequentially with 2.8 mM glucose, 16.8 mM glucose and finally 30 mM KCl to induce insulin secretion. Islet genomic DNA was quantified for normalization of ELISA insulin measurements to DNA content. n=5 technical replicates per condition and genotype. Data show mean ± SEM. Note that islet dispersion necessary for lentiviral transduction decreased the overall responsiveness of purified islets compared to intact islets. Insulin secretion by *Rnls* mutant islet cells was not significantly different from that of control (NT) islets. **d**: Growth curves for NIT-1 WT, control (NT gRNA) and *Rnls*^mut^ cells seeded in 96-well plates at 50,000 cells/well over one week. Culture media were refreshed in every 2 days. Cell growth was measured on days 0, 3 and 7 using the CellTiter-Glo luminescence Cell Viability Assay (Promega). Growth rates were not significantly different as calculated by one-way ANOVA with Dunnett's multiple comparisons test. n=3 technical replicates per genotype. Data show mean ± SEM.

a

b

c

Extended Data Fig. 3. *Rnls* **mutation prevents autoimmune killing but not allo-rejection of NIT-1 beta cells.**

Control and *Rnls*mut NIT-1 cells (10^7) carrying a luciferase reporter were implanted on opposing flanks of NOD.*scid* (**a**) or C57BL/6 mice (**b,c**). **a:** Graft bioluminescence was measured on days 0 and 57 after transplantation of NIT-1 cells together with diabetogenic NOD splenocytes (as in Fig. 2). **b,c:** Graft bioluminescence was measured on days 0, 4 and 7 after transplantation. Representative bioluminescence images (**b**) and relative luminescence

of grafts over time (**c**) are shown (n=3). Data represent mean ± SEM. Both control and mutant grafts were destroyed by allo-rejection within a week.
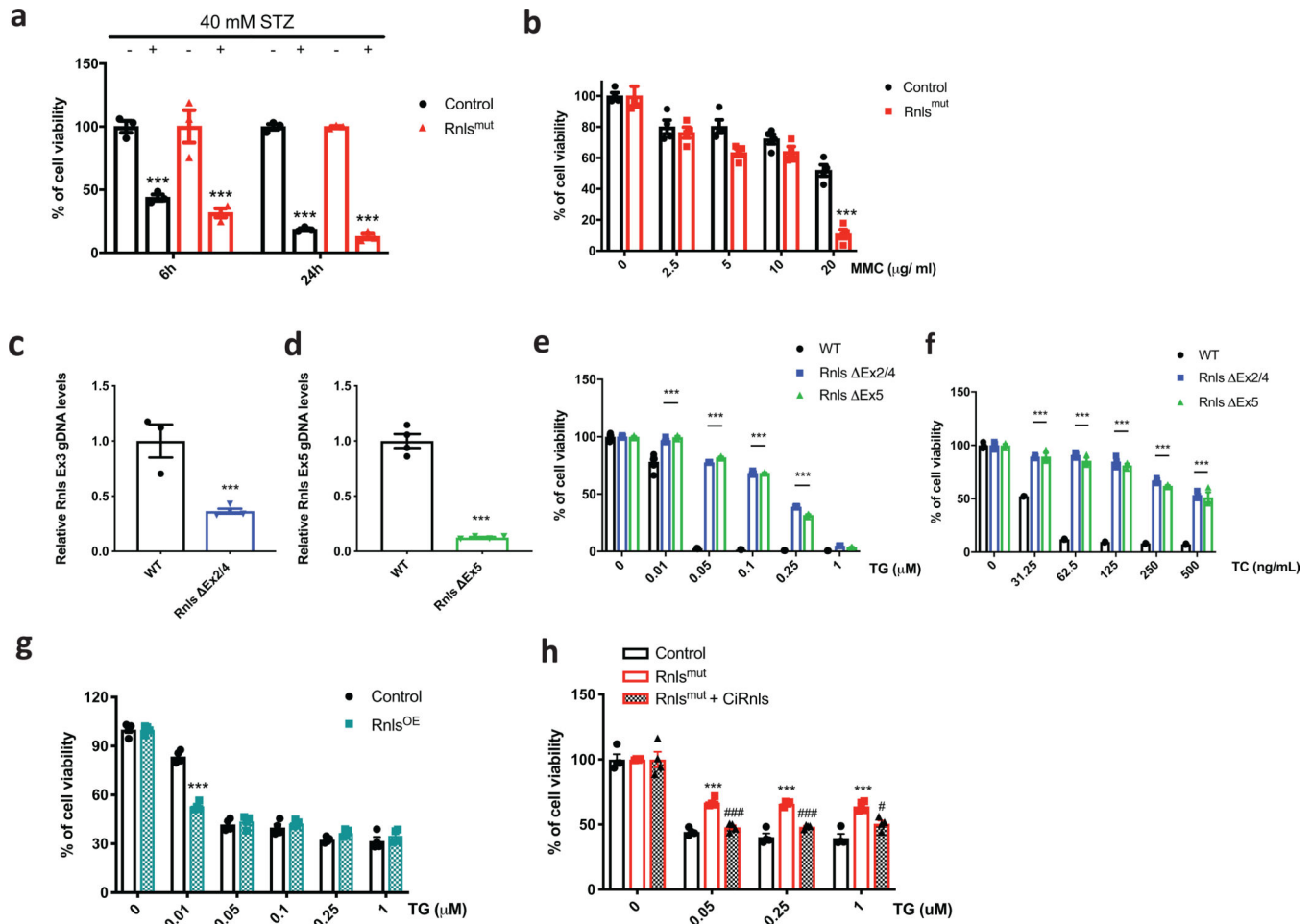
Extended Data Fig. 4. *Rnls* expression modulates the sensitivity to ER stress-induced cell death but not to ER stress-unrelated apoptosis.

a: Viability of *Rnls*mut and control NIT-1 cells at 6 h and 24 h after treatment with 40 mM streptozotocin (STZ) (n=3 technical replicates). **b:** NIT-1 cell viability 48 h after mitomycin C (MMC) at the indicated concentration (n=3 technical replicates). *** $P < 0.0001$, calculated by two-way ANOVA with Sidak's multiple comparisons test. **c-f:** *Rnls* knockout NIT-1 cell lines were generated by deleting either exons 2–4 or exon 5. Deletion efficiency was confirmed by qPCR of genomic DNA. *Rnls* Ex2/4 cells showed ~60% deletion of exons 2–4 genomic DNA qPCR (**c**) while *Rnls* Ex5 cells showed ~87% deletion of exon 5 (**d**). Cell viability of *Rnls* deficient cells was measured 72 h after thapsigargin (TG, **e**) and tunicamycin (TC, **f**) treatment. *** $P < 0.0001$, calculated by unpaired t-test (**c,d**) and two-way ANOVA with Sidak's multiple comparisons test (**e,f**). **g,h:** Overexpression of *Rnls* in WT NIT-1 cells increased sensitivity to low dose-TG-induced killing (**g**). n=4 technical replicates per group. *** $P < 0.0001$, calculated by two-way ANOVA with Sidak's multiple comparisons test. CRISPR-immune *Rnls* (CiRnls) expressed in *Rnls*mut cells restored sensitivity to TG-induced killing (**h**). n=4 technical replicates per group. ***$P < 0.001$, #$P =$

0.0138, [###]$P = 0.0002$, 0.0005 for 0.05 and 0.25 TG(μM) respectively, calculated by two-way ANOVA with Sidak's multiple comparisons test. *Comparison of control vs. *Rnls*[mut] cells; #comparison of *Rnls*[mut] vs. *Rnls*[mut] + *CiRnls* cells. All data represent mean ± SEM.
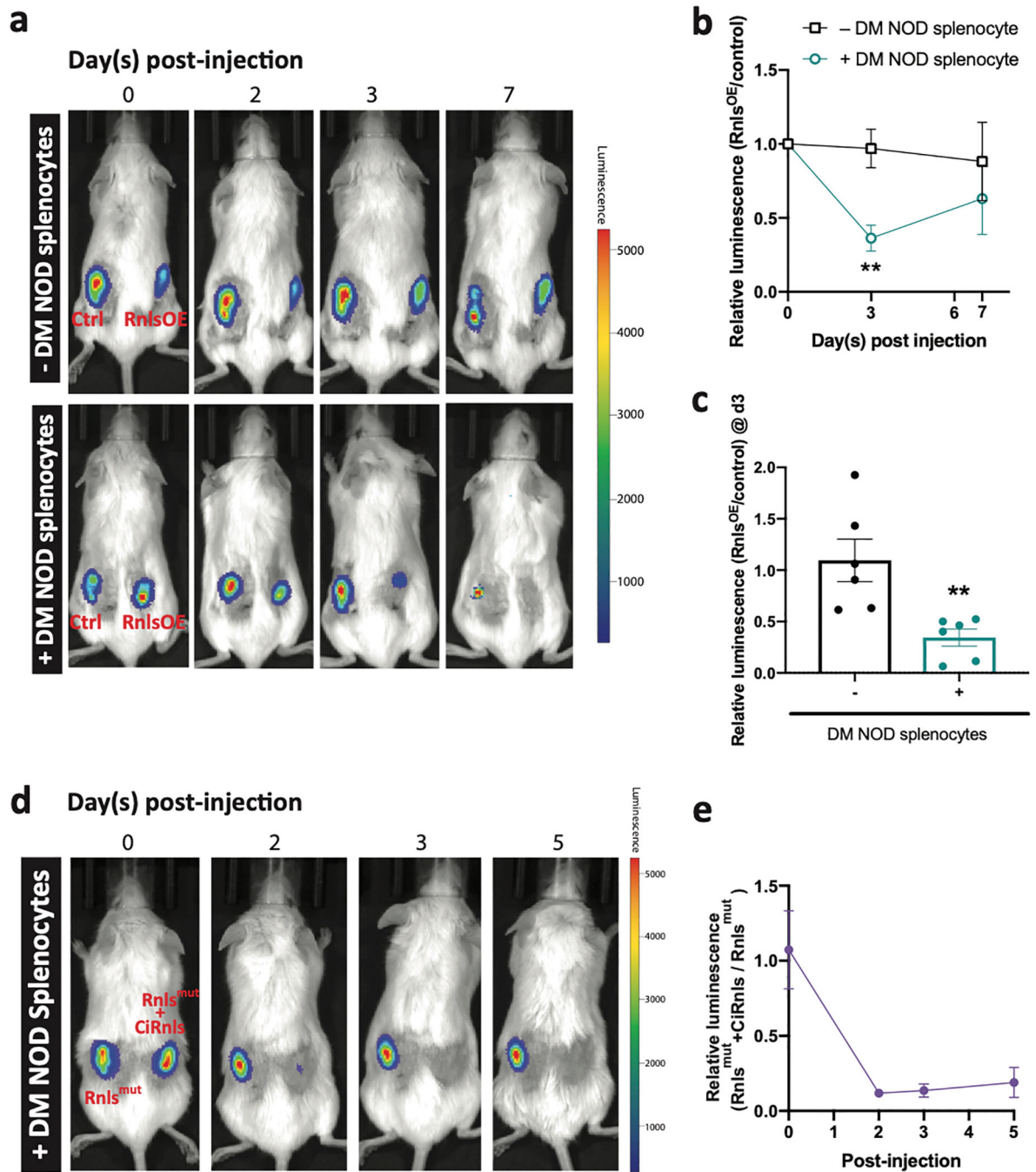
Extended Data Fig. 5. *Rnls* overexpression increases sensitivity to autoimmune killing *in vivo*. a-c: Control (WT) and *Rnls* overexpressing (Rnls[OE]) NIT-1 cells carrying a luciferase reporter were implanted on opposing flanks of NOD.*scid* mice. Some graft recipients were also injected intravenously with splenocytes from diabetic NOD mice (DM NOD

splenocytes). Graft bioluminescence was imaged on days 0, 2, 3 and 7 (**a**). The relative luminescence of Rnls^{OE} and control grafts over time, normalized to day 0, is shown in (**b**). Data for all mice analyzed on day 3 is shown in (**c**). Rnls^{OE} graft were more sensitive to autoimmune killing as evidenced by more rapid loss of luminescence. By day 7, both control and Rnls^{OE} grafts were killed to ~90% (data not shown), resulting in a similar relative luminescence level. n=6 mice (each with two grafts). Data represent mean ± SEM, **$P <$ 0.0022, calculated by two-sided Mann-Whitney test. **d,e:** *Rnls*^{mut} NIT-1 cells and *Rnls*^{mut} cells expressing the CRISPR-immune *Rnls* transgene (CiRnls), all carrying a luciferase reporter, were implanted on opposing flanks of NOD.*scid* mice. Graft recipients were also injected intravenously with splenocytes from diabetic (DM) NOD mice. Graft bioluminescence was imaged on days 0, 2, 3 and 5 post-injection (**d**). Relative luminescence of paired grafts over time normalized to day 0 is shown in (**e**). n=5 mice. Data represent mean ± SEM.
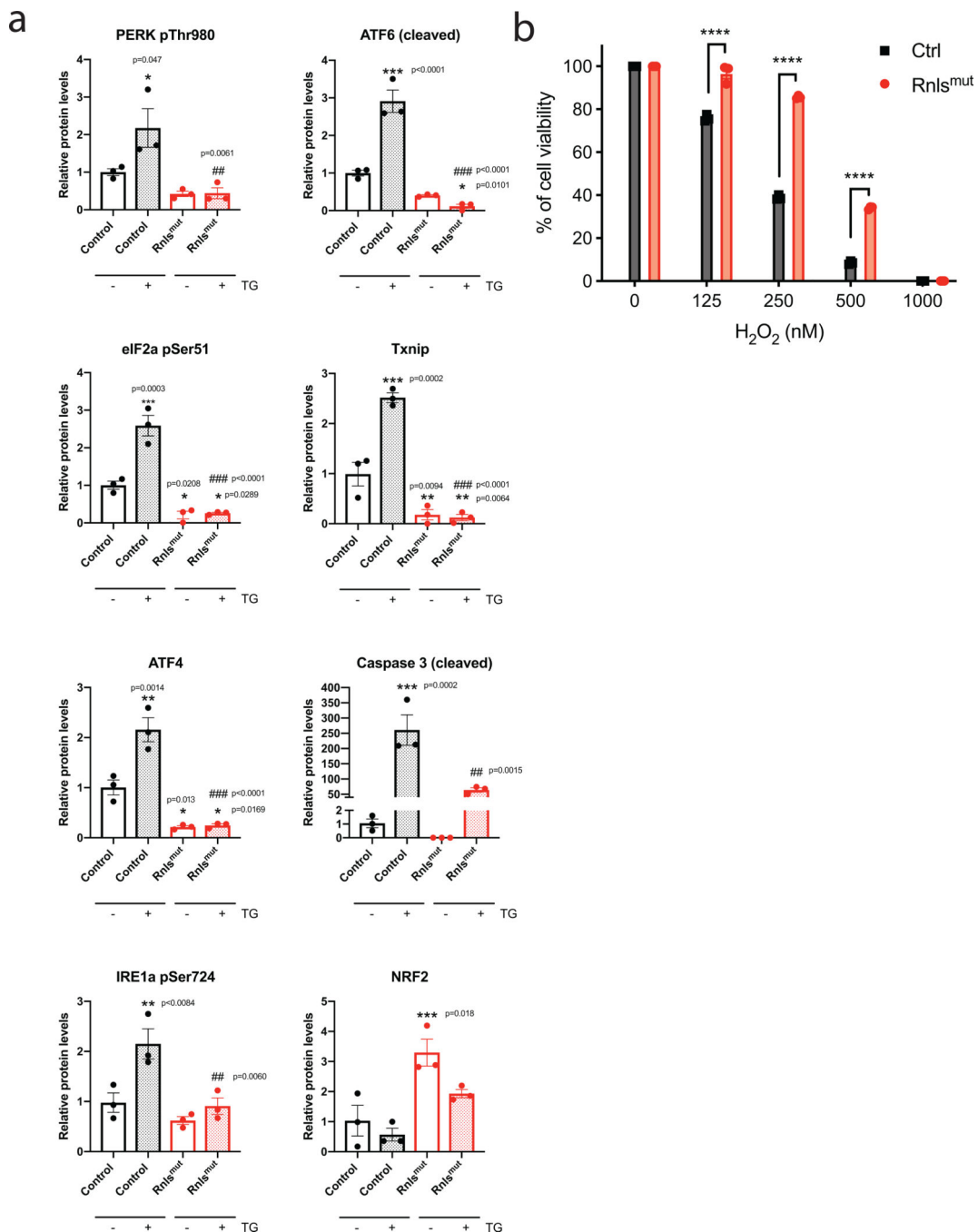
Extended Data Fig. 6. *Rnls* deficiency diminishes the UPR following ER stress and protects against oxidative stress.

a: Quantification of Western blot data shown in Figure 4e. Images were obtained and quantified using a C-DiGit scanner and the Image Studio software (LI-COR Biosciences). n=3 per group. Data show mean ± SEM, *# $P < 0.05$, **## $P < 0.01$, ***### $P < 0.001$, calculated by one-way ANOVA with Dunnett's multiple comparisons test. *Comparison to control cells without TG treatment; #comparison to control cells with 5-hour TG treatment. **b:** Control (Ctrl) and *Rnls*mut NIT-1 cells were cultured overnight with or without hydrogen

peroxide (H_2O_2) at the indicated concentrations. Cell viability was assessed using the CellTiter-Glo luminescence Cell Viability Assay. Data show mean ± SEM of triplicate cultures and are representative of three independent experiments. **** P<0.0001, calculated by two-way ANOVA with Sidak's multiple comparison test.
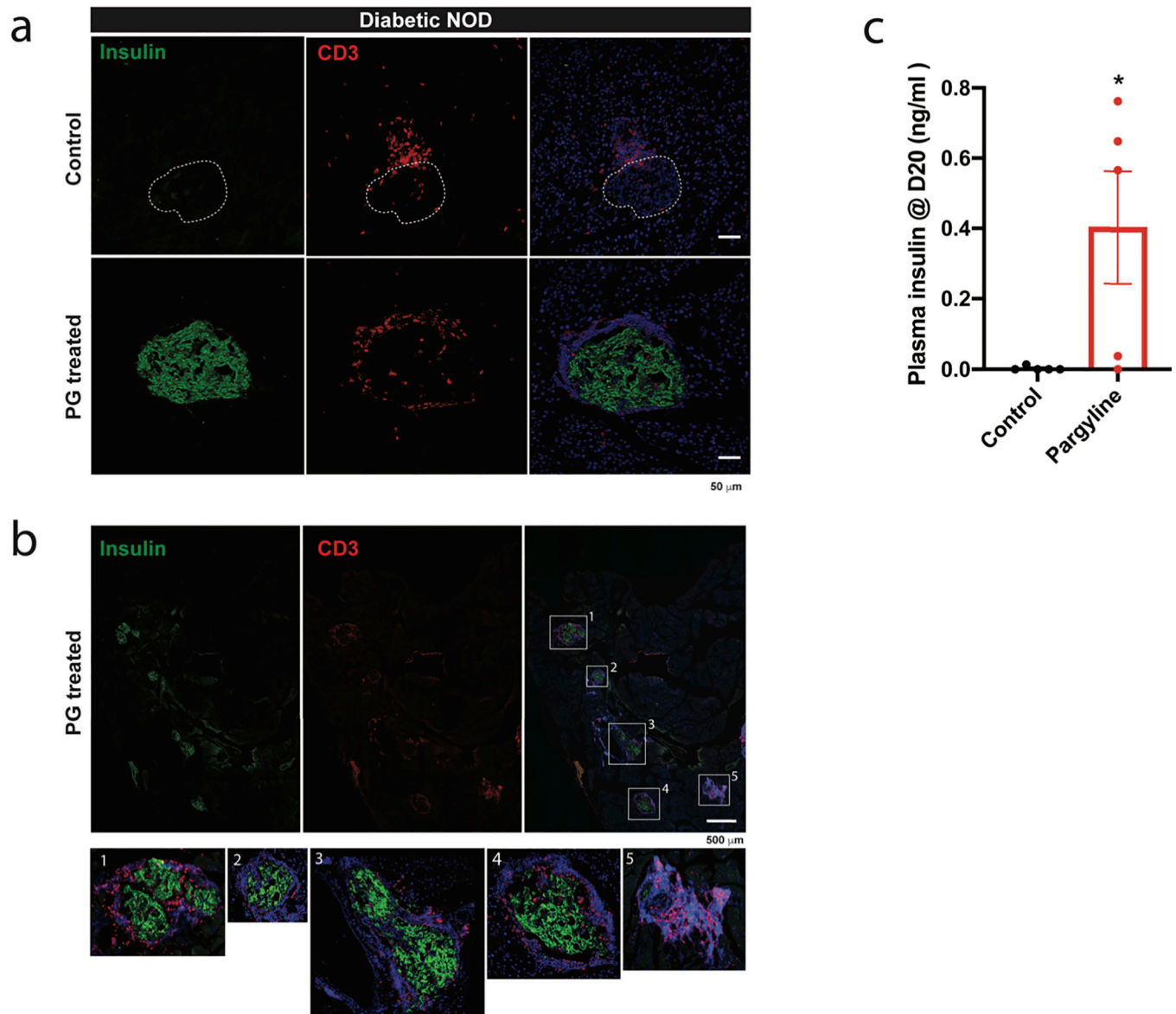
**Extended Data Fig. 7. Pargyline treatment preserves insulin expression in NOD mice with long-duration diabetes**

Pancreases were isolated from control and pargyline-treated diabetic NOD mice described in Figure 6 that were euthanised at day 20 post beta cell-transplantation. Pancreatic sections were stained with anti-insulin (DAKO, #A0564), anti-CD3 (Bio-rad, #MCA500), and DNA dye Hoechst 33342 (Invitrogen, #H3570). Goat anti-guinea pig Alexa Flour 488 and donkey anti-rat Alexa Flour 594 secondary antibodies (Thermo Fisher Scientific, #A11073 and #A21209) were used to detect insulin and CD3 antibodies, respectively. **a:** Representative

images of individual islets, taken with a Zeiss LSM710NLO confocal microscope. **b:** Representative pancreas section from a pargyline (PG)-treated animal scanned using a Thermo Fisher Scientific EVOS FL Auto imaging system. Five islets were identified on the section: islets #1–4 showed many insulin-expressing cells, islet #5 had no remaining insulin-expressing cells. No significant insulin staining was detectable in the pancreas of untreated mice (not shown). **c:** Plasma insulin levels at day 20 post-transplantation in diabetic mice with a NIT-1 beta cell graft that were treated or not with PG. Data show mean ± SEM of n=5 mice per group and are representative of two independent experiments, * $P = 0.0367$, calculated by two-sided unpaired t-test.
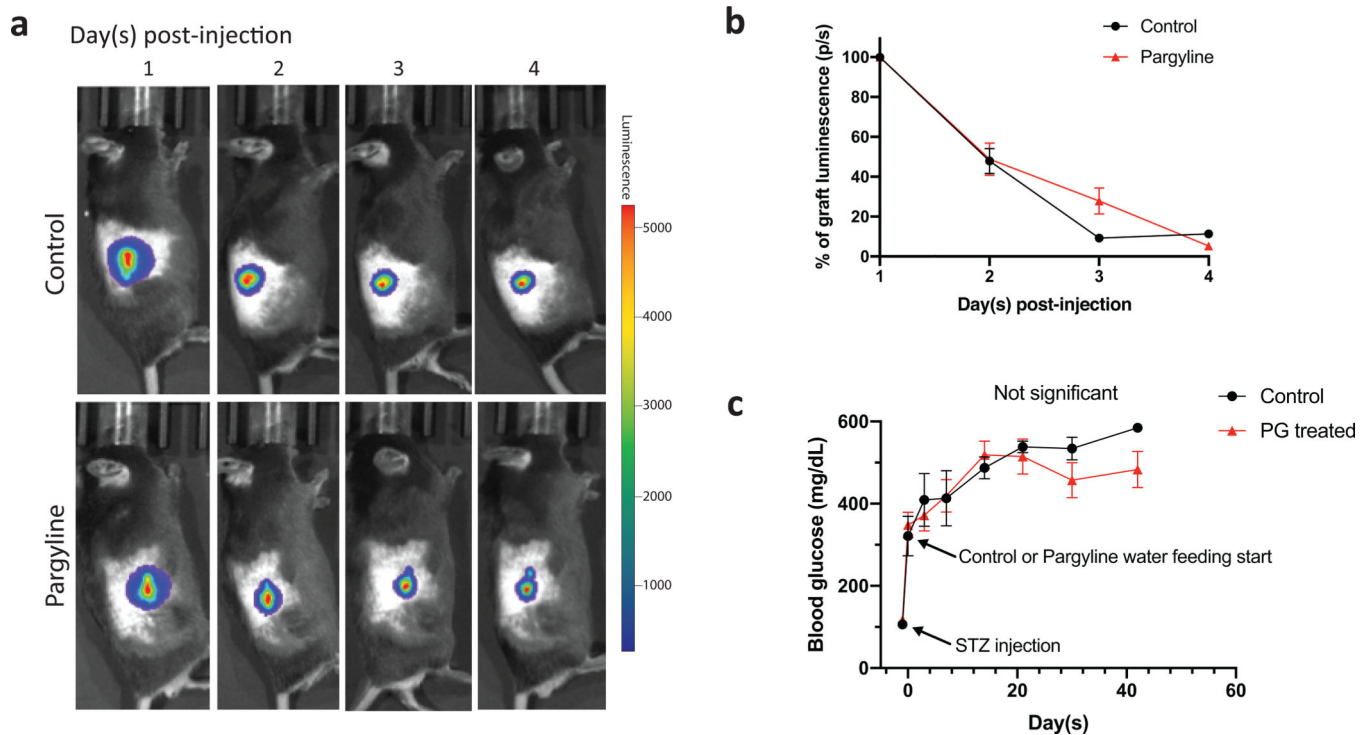
Extended Data Fig. 8. Pargyline treatment does not prevent beta cell destruction after allo-transplantation and has no glucose-lowering effect on its own.

a, b: Wild-type NIT-1 cells (10^7) carrying a luciferase reporter were implanted into C57BL/6 mice that were treated or not with oral pargyline via addition to the drinking water. Graft bioluminescence was measured on days 1, 2, 3 and 4 after transplantation. Representative bioluminescence images (**a**) and relative luminescence of grafts over time (**b**) are shown. Data show mean ± SEM for n=3 mice per group. **c:** Pargyline did not decrease hyperglycemia in C57BL/6 mice rendered diabetic by streptozotocin (STZ) injection (150mg/kg). Data show mean ± SEM for n=5 mice (control) and n=9 (pargyline).
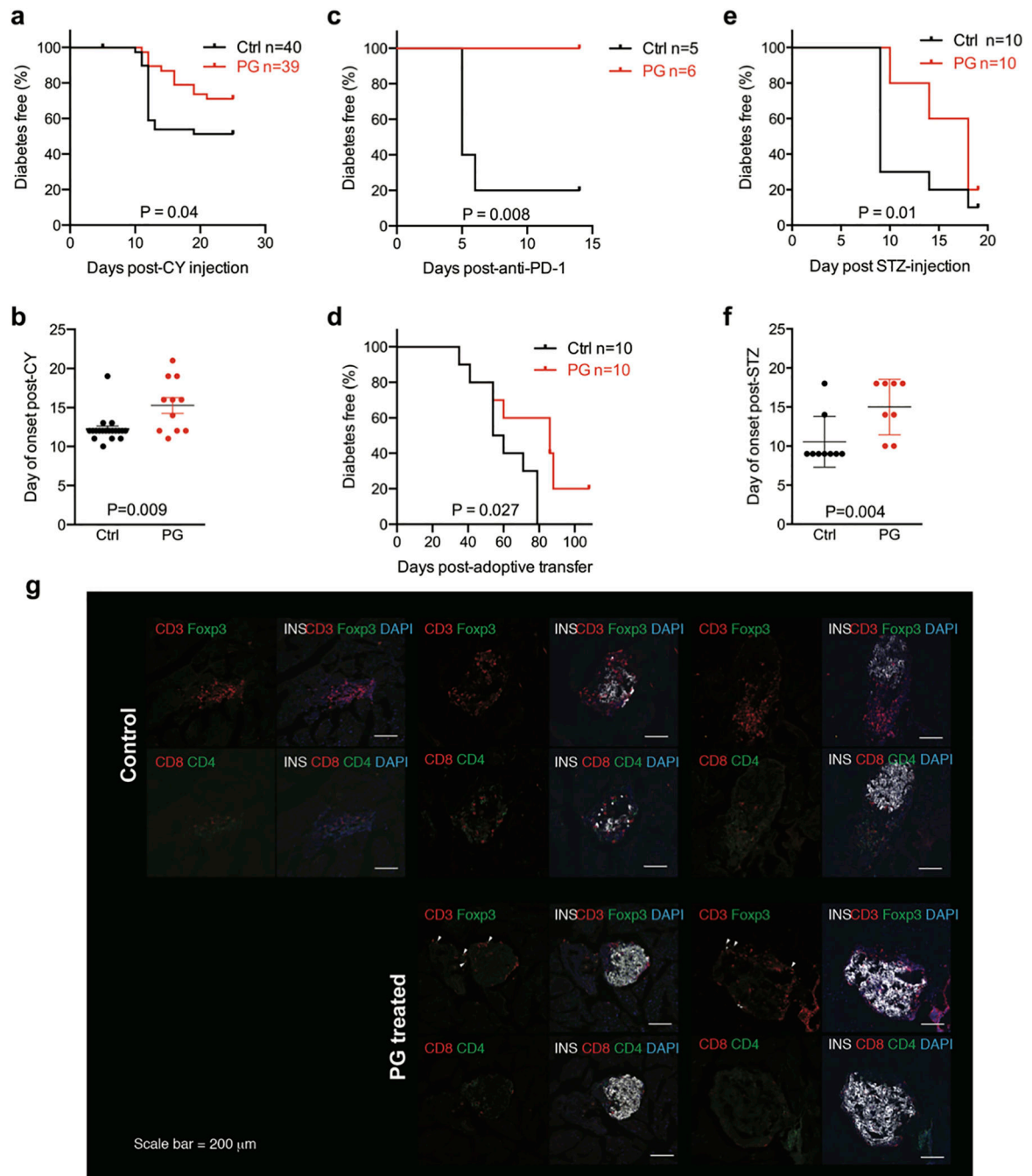
Extended Data Fig. 9. Pargyline prevents or delays diabetes in multiple mouse models for T1D.
a: Diabetes frequency after cyclophosphamide injection of NOD mice fed with control water (Ctrl, n=40) or water containing pargyline (PG, n=39). **b**: Day of disease onset in mice that developed diabetes after cyclophosphamide injection (Ctrl n=19, PG n=11). **c:** Diabetes frequency in NOD mice injected with blocking anti-PD-1 antibody with (n=6) or without (n=5) oral PG treatment (as in **a**). **d**: Diabetes frequency in NOD.*scid* mice transplanted with splenocytes (10^7 cells) from diabetic NOD mice and treated with or without PG (n=10 per group). **e,f:** Diabetes frequency (n=10 per group) and day of disease onset (ctrl n= 9, PG

Cai et al. Page 26

n=8) in C57BL/6 mice treated with multiple low doses of streptozotocin. Kaplan-Meier survival curves were compared by Log-rank test (**a,c,d and e**). Time of disease onset is shown as mean ± SEM and was compared by Mann-Whitney test (**b,f**). Exact P values are shown. **g:** Insulin and T cell marker staining in pancreas sections from NOD mice two weeks after anti-PD-1 injection, with or without PG treatment.

a

b

c
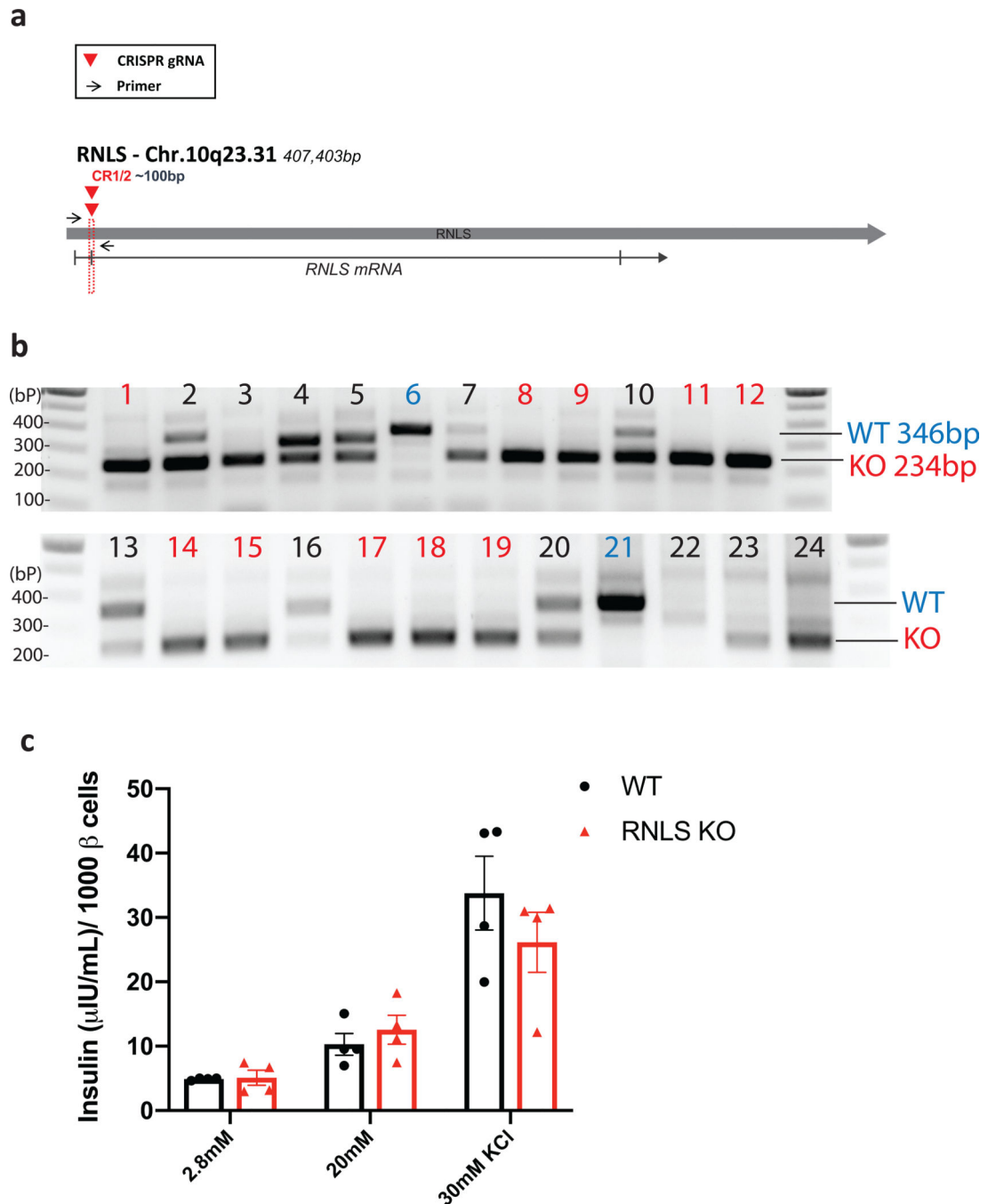
Extended Data Fig. 10. Design, genotyping and phenotyping of *RNLS* deletion in human SC-beta cells.

Nat Metab. Author manuscript; available in PMC 2021 January 27.

a: *RNLS* dual-gRNA design for the generation of *RNLS* knockout (KO) human induced pluripotent stem cells (SC). **b:** Genotyping of SC clones. CRISPR targeted clones were genotyped by PCR that was repeated for confirmation for all mutant clones, and individual mutations were verified by sequencing. Clone 1 was used as *RNLS* KO in this study and carried a 112bp deletion on both alleles. **c:** Glucose stimulated insulin secretion by SC-beta cells differentiated from WT or *RNLS* KO isogenic SC clones. Data in **c** show mean insulin secretion from four independent SC-beta cell batches, each measured in triplicate, following stimulation with 2.8mM glucose, 20mM glucose, or 30mM potassium chloride (KCl). Data show mean ± SEM for n=4 technical replicates per condition and genotype.

Supplementary Material

Refer to Web version on PubMed Central for supplementary material.

Acknowledgements

References

1. Atkinson MA, Roep BO, Posgai A, Wheeler DCS & Peakman M The challenge of modulating β-cell autoimmunity in type 1 diabetes. Lancet Diabetes Endocrinol. 7, 52–64 (2019). [PubMed: 30528099]

2. Odorico J et al. Report of the Key Opinion Leaders Meeting on Stem Cell-derived Beta Cells. Transplantation 102, 1223–1229 (2018). [PubMed: 29781950]

3. Herold KC et al. An Anti-CD3 Antibody, Teplizumab, in Relatives at Risk for Type 1 Diabetes. N. Engl. J. Med. NEJM 381, 603–613 (2019). [PubMed: 31180194]

4. Kroger CJ, Clark M, Ke Q & Tisch RM Therapies to suppress β cell autoimmunity in type 1 diabetes. Frontiers in Immunology 9, (2018).

5. Han X et al. Generation of hypoimmunogenic human pluripotent stem cells. Proc. Natl. Acad. Sci. 116, 10441–10446 (2019). [PubMed: 31040209]

6. Deuse T et al. Hypoimmunogenic derivatives of induced pluripotent stem cells evade immune rejection in fully immunocompetent allogeneic recipients. Nat. Biotechnol. 37, 252–258 (2019). [PubMed: 30778232]

7. Hamaguchi K, Gaskins HR & Leiter EH NIT-1, a pancreatic beta-cell line established from a transgenic NOD/Lt mouse. Diabetes 40, 842–9 (1991). [PubMed: 1647994]

8. Pearson JA, Wong FS & Wen L The importance of the Non Obese Diabetic (NOD) mouse model in autoimmune diabetes. J. Autoimmun. 66, 76–88 (2016). [PubMed: 26403950]

9. Sanjana NE, Shalem O & Zhang F Improved vectors and genome-wide libraries for CRISPR screening. Nat. Methods 11, 783–784 (2014). [PubMed: 25075903]

10. Barrett JC et al. Genome-wide association study and meta-analysis find that over 40 loci affect risk of type 1 diabetes. Nat. Genet. 41, 703–7 (2009). [PubMed: 19430480]

11. Howson JMM et al. Evidence of gene-gene interaction and age-at-diagnosis effects in type 1 diabetes. Diabetes 61, 3012–7 (2012). [PubMed: 22891215]

12. Haskins K, Portas M, Bergman B, Lafferty K & Bradley B Pancreatic islet-specific T-cell clones from nonobese diabetic mice. Proc. Natl. Acad. Sci. 86, 8000–8004 (1989). [PubMed: 2510155]

13. Katz JD, Wang B, Haskins K, Benoist C & Mathis D Following a diabetogenic T cell from genesis through pathogenesis. Cell 74, 1089–100 (1993). [PubMed: 8402882]

14. Marré ML et al. Inherent ER stress in pancreatic islet β cells causes self-recognition by autoreactive T cells in type 1 diabetes. J. Autoimmun. 72, 33–46 (2016). [PubMed: 27173406]

15. Clark AL & Urano F Endoplasmic reticulum stress in beta cells and autoimmune diabetes. Curr. Opin. Immunol. 43, 60–66 (2016). [PubMed: 27718448]

16. Ozcan U et al. Endoplasmic Reticulum Stress Links Obesity, Insulin Action, and Type 2 Diabetes. Science 306, 457–461 (2004). [PubMed: 15486293]

17. Izumi T et al. Dominant negative pathogenesis by mutant proinsulin in the Akita diabetic mouse. Diabetes 52, 409–16 (2003). [PubMed: 12540615]

18. Kracht MJL et al. Autoimmunity against a defective ribosomal insulin gene product in type 1 diabetes. Nat. Med. 23, 501–507 (2017). [PubMed: 28263308]

19. Marre ML et al. Modifying Enzymes Are Elicited by ER Stress, Generating Epitopes That Are Selectively Recognized by CD4 $^+$ T Cells in Patients With Type 1 Diabetes. Diabetes 67, 1356–1368 (2018). [PubMed: 29654212]

20. Sidney J et al. Low HLA binding of diabetes-associated CD8+ T-cell epitopes is increased by post translational modifications. BMC Immunol. 19, 12 (2018). [PubMed: 29562882]

21. Thomaidou S et al. Beta-Cell Stress Shapes CTL Immune Recognition of Preproinsulin Signal Peptide by Post-Transcriptional Regulation of Endoplasmic Reticulum Aminopeptidase 1. Diabetes db190984 (2020). doi:10.2337/db19-0984

22. Cardozo AK et al. Cytokines downregulate the sarcoendoplasmic reticulum pump Ca2+ ATPase 2b and deplete endoplasmic reticulum Ca2+, leading to induction of endoplasmic reticulum stress in pancreatic beta-cells. Diabetes 54, 452–461 (2005). [PubMed: 15677503]

23. Cox JS, Shamu CE & Walter P Transcriptional induction of genes encoding endoplasmic reticulum resident proteins requires a transmembrane protein kinase. Cell 73, 1197–206 (1993). [PubMed: 8513503]

24. Harding HP, Zhang Y & Ron D Protein translation and folding are coupled by an endoplasmic-reticulum-resident kinase. Nature 397, 271–274 (1999). [PubMed: 9930704]

25. Yoshida H, Haze K, Yanagi H, Yura T & Mori K Identification of the *cis* -Acting Endoplasmic Reticulum Stress Response Element Responsible for Transcriptional Induction of Mammalian Glucose-regulated Proteins. J. Biol. Chem. 273, 33741–33749 (1998). [PubMed: 9837962]

26. Oyadomari S et al. Targeted disruption of the Chop gene delays endoplasmic reticulum stress–mediated diabetes. J. Clin. Invest. 109, 525–532 (2002). [PubMed: 11854325]

27. Minn AH, Hafele C & Shalev A Thioredoxin-Interacting Protein Is Stimulated by Glucose through a Carbohydrate Response Element and Induces β-Cell Apoptosis. Endocrinology 146, 2397–2405 (2005). [PubMed: 15705778]

28. Oslowski CM et al. Thioredoxin-Interacting Protein Mediates ER Stress-Induced β Cell Death through Initiation of the Inflammasome. Cell Metab. 16, 265–273 (2012). [PubMed: 22883234]

29. Kensler TW, Wakabayashi N & Biswal S Cell survival responses to environmental stresses via the Keap1-Nrf2-ARE pathway. Annu. Rev. Pharmacol. Toxicol. 47, 89–116 (2007). [PubMed: 16968214]

30. Moran GR The catalytic function of renalase: A decade of phantoms. Biochim. Biophys. Acta - Proteins Proteomics 1864, 177–186 (2016).

31. Beaupre BA, Hoag MR, Roman J, Försterling FH & Moran GR Metabolic Function for Human Renalase: Oxidation of Isomeric Forms of β-NAD(P)H that Are Inhibitory to Primary Metabolism. Biochemistry 54, 795–806 (2015). [PubMed: 25531177]

32. Milani M et al. FAD-Binding Site and NADP Reactivity in Human Renalase: A New Enzyme Involved in Blood Pressure Regulation. J. Mol. Biol. 411, 463–473 (2011). [PubMed: 21699903]

33. Taylor JD, Wykes AA, Gladish YC & Martin WB New Inhibitor of Monoamine Oxidase. Nature 187, 941–942 (1960). [PubMed: 13775618]

34. Ansari MJ et al. The programmed death-1 (PD-1) pathway regulates autoimmune diabetes in nonobese diabetic (NOD) mice. J. Exp. Med. 198, 63–69 (2003). [PubMed: 12847137]

35. Like AA & Rossini AA Streptozotocin-induced pancreatic insulitis: new model of diabetes mellitus. Science 193, 415–417 (1976). [PubMed: 180605]

36. Roep BO Are insights gained from NOD mice sufficient to guide clinical translation? Another inconvenient truth. Ann. N. Y. Acad. Sci. 1103, 1–10 (2007). [PubMed: 17376838]

37. Pagliuca FW et al. Generation of Functional Human Pancreatic β Cells In Vitro. Cell 159, 428–439 (2014). [PubMed: 25303535]

38. Wang L et al. Renalase Prevents AKI Independent of Amine Oxidase Activity. J. Am. Soc. Nephrol. 25, 1226–1235 (2014). [PubMed: 24511138]

39. Wang L, Velazquez H, Chang J, Safirstein R & Desir GV Identification of a receptor for extracellular renalase. PLoS One 10: e0122932 (2015) [PubMed: 25906147]

40. Kolodecik TR et al. The Serum Protein Renalase Reduces Injury in Experimental Pancreatitis. J. Biol. Chem. 292, 21047–21059 (2017). [PubMed: 29042438]

41. Veres A et al. Charting cellular identity during human in vitro β-cell differentiation. Nature 569, 368–373 (2019). [PubMed: 31068696]

42. Sanjana NE, Shalem O, Zhang F Improved vectors and genome-wide libraries for CRISPR screening. Nat. Methods. 11, 783–784, (2014). [PubMed: 25075903]

43. Joung J, Konerman S, Gootenberg J, Abudayyeh O, Platt R, Brigham M, Sanjana N, Zhang F Genome-scale CRISPR-Cas9 knockout and transcriptional activation screening. Nat. Protoc. 12, 828–863, (2017). [PubMed: 28333914]

44. Schuster C, Jonas F, Zhao F, Kissler S Peripherally induced regulatory T cells contribute to the control of autoimmune diabetes in the NOD mouse model. Eur. J. Immunol. 48, 1211–1216, (2018). [PubMed: 29604048]

45. Shalem O, Sanjana N, Hartenian E, Shi X, Scott D, Heckl D, Ebert B, Root D, Doench J, Zhang F Genome-scale CRISPR-Cas9 knockout screening in human cells. Science 343, 84–87, (2014). [PubMed: 24336571]

46. Cao J, Wu L, Zhang SM, Lu M, Cheung WK, Cai W, Gale M, Xu Q, Yan Q An easy and efficient inducible CRISPR/Cas9 platform with improved specificity for multiple gene targeting. Nucleic Acids Res. 44, e149, (2016). [PubMed: 27458201]

47. Kuznetsova A, Yu Y, Hollister-Lock J, Opare-Addo L, Rozzo A, Sadagurski M, Norquay L, Reed JE, El Khattabi I, Bonner-Weir S, Weir GC, Sharma A, White MF Trimeprazine increases IRS2 in human islets and promotes pancreatic beta cell growth and function in mice. JCI Insight 1, pii: e80749 (2016) [PubMed: 27152363]

48. Milani M, Ciriello F, Baroni S, Pandini V, Canevari G, Bolognesi M, Aliverti A FAD-binding site and NADP reactivity in human renalase: a new enzyme involved in blood pressure regulation. J. Mol. Biol. 411, 463–473 (2011). [PubMed: 21699903]

49. Binda C, Hubalek F, Li M, Herzig Y, Sterling J, Edmonson DE, Mattevi A Binding of rasagiline-related inhibitors to human monoamine oxidases: a kinetic and crystallographic analysis. J. Med. Chem. 48, 8148–8154 (2005). [PubMed: 16366596]

50. Sastry GM, Adzhigirey M, Day T, Annabhimoju R, Sherman W Protein and ligand preparation: Parameters, protocols, and influence on virtual screening enrichments. J. Comput. Aided Mol. Des, 27, 221–234 (2013). [PubMed: 23579614]

51. Bowers KJ, Chow DE, Xu H, Dror RO, Eastwood MP, Gregersen BA, Kelpeis JL, Kolossvary I, Moraes MA, Sacerdoti FD, Salmon JK, Shan Y, Shaw DE Scalable Algorithms for Molecular Dynamics Simulations on Commodity Clusters. Proceedings of the 2006 ACM/IEEE Conference on Supercomputing (SC06), p 43 (2006).
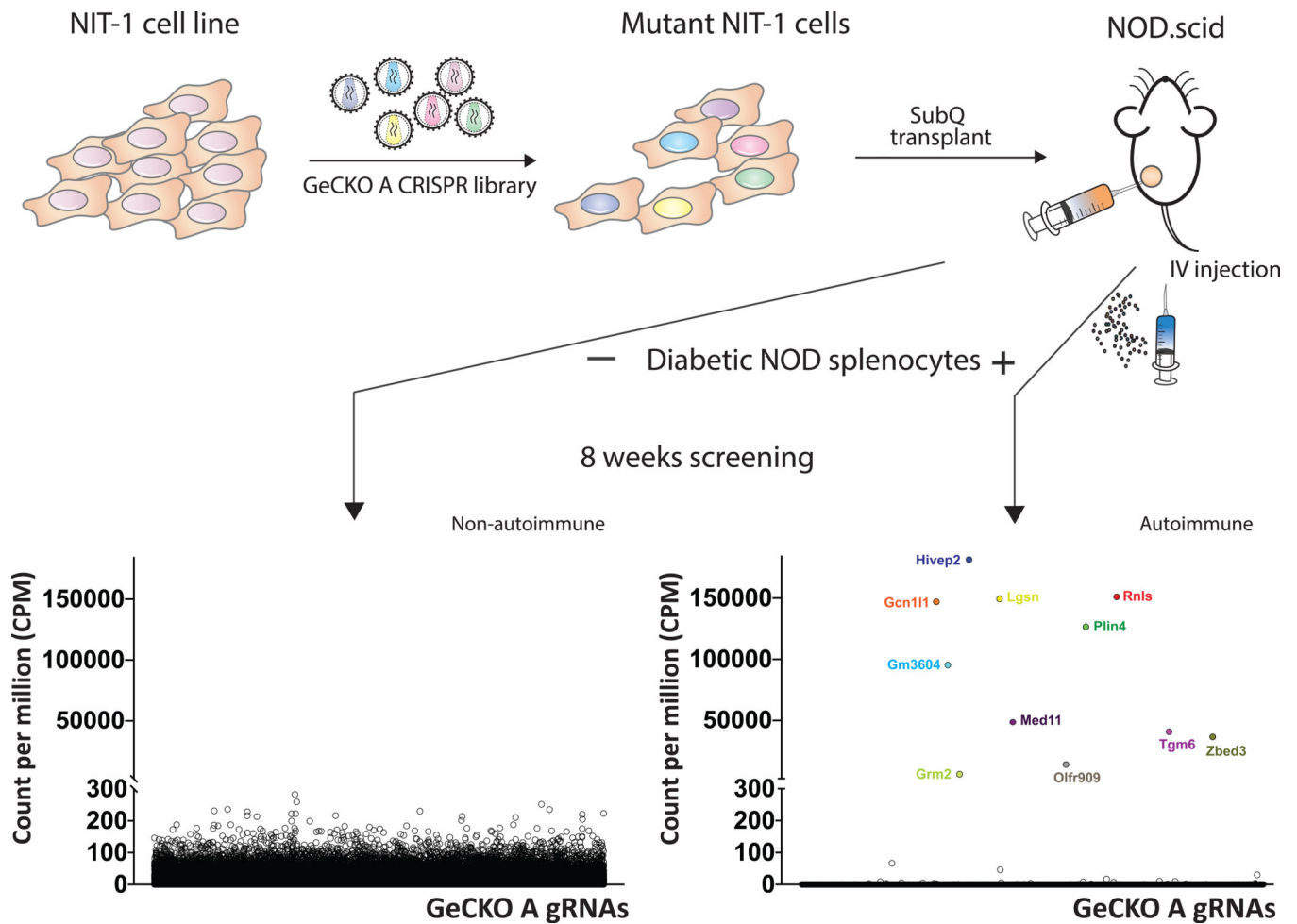
Fig. 1. Genome-scale CRISPR/Cas9 screen identifies *Rnls* as a modifier of beta cell survival in the NOD mouse model.

NIT-1 cells (10^7) transduced with the mouse GECKO A CRISPR lentiviral library (MOI=0.3) and selected with puromycin were implanted subcutaneously (SubQ) into NOD.*scid* mice, with or without intravenous injection of 10^7 splenocytes from diabetic NOD mice. After 8 weeks, NIT-1 grafts were retrieved from recipients with (autoimmune) and without (non-autoimmune) splenocyte co-injection. Next-generation sequencing of gRNAs present in surviving grafts identified *Rnls* gRNA (MGLibA_46009, 5'-CTACTCCTCTCGCTATGCTC-3') as one of only 11 gRNAs detected at high frequency in mice with beta cell autoimmunity.
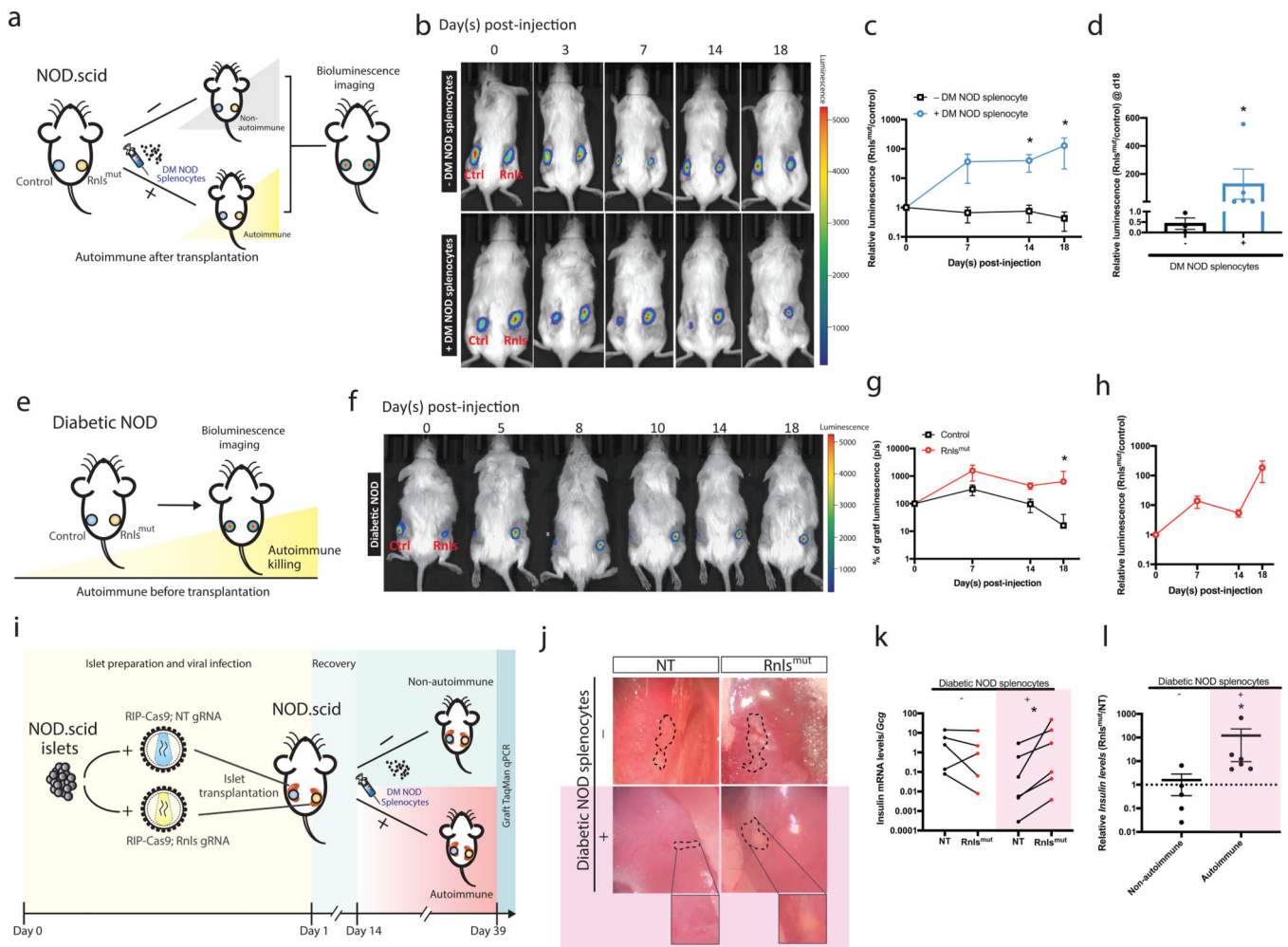
Fig. 2. *Rnls* mutation protects NIT-1 and primary NOD beta cells against autoimmune destruction.

a: Experimental approach used to test NIT-1 beta cell survival after transplantation and induction of autoimmunity. Control and *Rnls*^{mut} NIT-1 cells (10^7) carrying a luciferase reporter were implanted on opposite flanks of NOD.*scid* mice. Autoimmunity was induced by injection of 10^7 splenocytes from diabetic (DM) NOD mice. **b:** Representative images of graft luminescence at days 0, 3, 7, 14 and 18 post-transplantation. **c,d:** Relative luminescence of paired *Rnls*^{mut} and control grafts over time (**c**) and at day 18 (**d**), normalized to the ratio on day 0. *P=0.0357 at days 14 and 18 post-transplantation. Data show mean ± SEM of n=5 (+splenocytes) and n=3 (-splenocytes) mice. **e:** Experimental approach used to test NIT-1 cell survival transplanted into diabetic NOD mice. Control (NT) and *Rnls*^{mut} NIT-1 cells (10^7) were implanted on opposing flanks of overtly diabetic NOD mice. **f:** Representative images of graft luminescence at day 0, 5, 8, 10, 14 and 18 post-transplantation. **g:** Proportion of remaining luminescence relative to day 0 (100%), *P=0.012. **h:** Relative luminescence of paired *Rnls*^{mut} and control grafts. Data show mean ± SEM of n=5 mice. **i:** Experimental approach used to test autoimmune killing of primary islet beta cells. NOD.*scid* islet cells transduced with lentivirus encoding a non-targeting (NT) control or *Rnls*-targeting gRNA and RIP-driven Cas9 endonuclease were transplanted under

the left and right kidney capsule, respectively, of the same NOD.*scid* recipients. Autoimmunity was induced as in (**a**). **j:** Representative images of transplanted islets on the explanted kidney at day 39. **k:** Quantification of insulin mRNA relative to glucagon (*Gcg*) mRNA in paired grafts from non-autoimmune (- splenocytes, n=5) and autoimmune (+ splenocytes, n=6) mice at day 39, *P=0.0312. **l:** Relative insulin expression in paired *Rnls*^{mut} and control (NT) grafts, *P=0.0173. Data represent mean ± SEM, calculated by two-sided Mann-Whitney test (**c-d**, **g-h**, **l**), and two-sided Wilcoxon signed-rank test (**k**). All data are representative of two or more independent experiments.
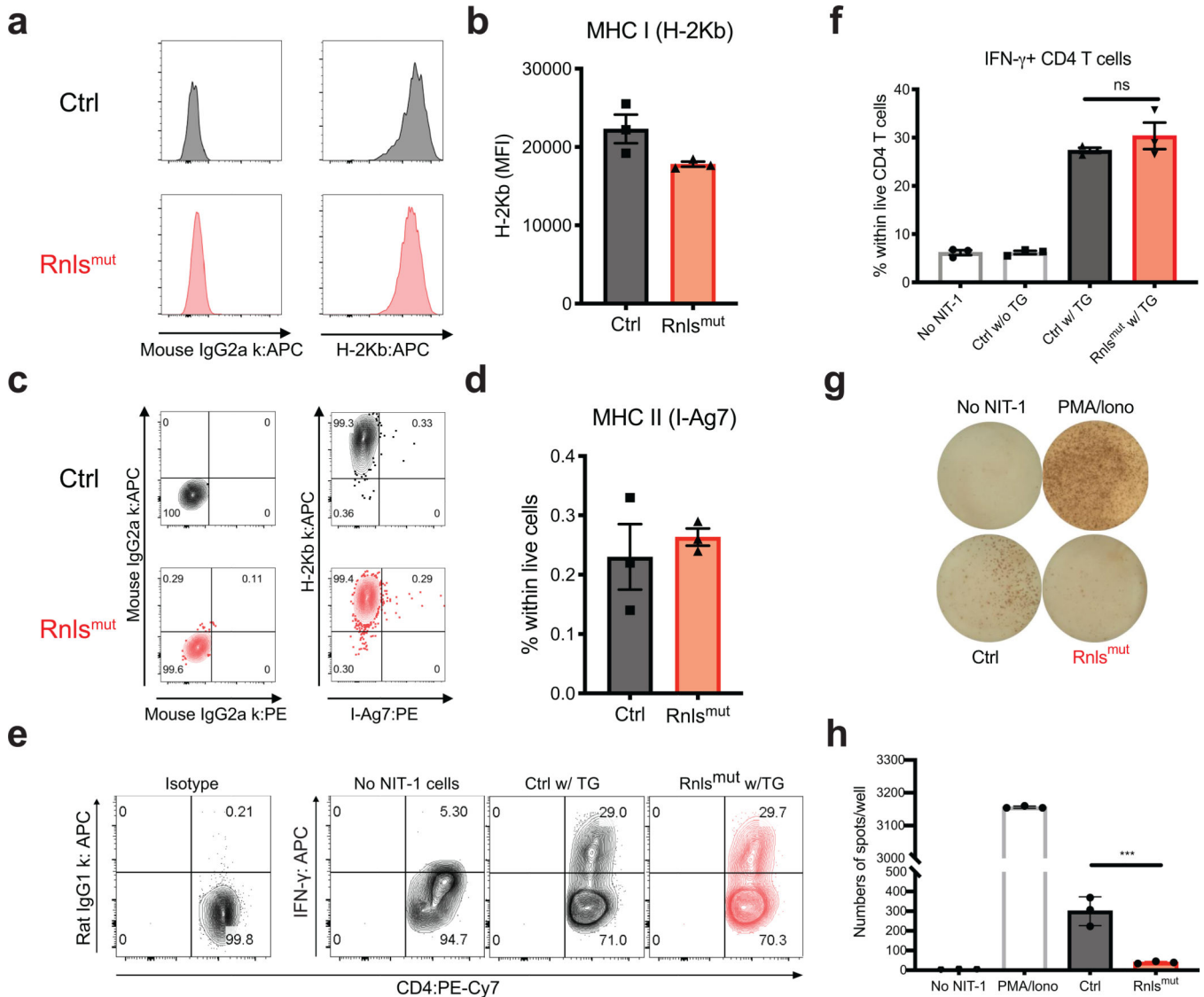
Fig. 3. *Rnls* deficiency diminishes immune recognition of beta cells.
a–d: Representative flow cytometry data (**a**,**c**) and summary data (**b**,**d**) for MHC-I (**a**,**b**, MFI: mean fluorescent intensity) and MHC-II (**c**,**d**, expressed as % MHC-II$^+$ cells) expression in control and *Rnls*^{mut} cells. Data are representative of three independent experiments. **e,f:** BDC2.5-TCR transgenic CD4$^+$ T cells were co-cultured with NIT-1 cells and irradiated splenocytes from NOD.*scid* mice. IFN-γ expression in CD4$^+$ T cells was measured at 24 h by flow cytometry. Representative (**e**) and combined data (**f**) from technical triplicates is shown. Data are representative of five independent experiments. **g,h:** ELISPOT measurement for the activation of polyclonal CD8$^+$ T cells from a diabetic NOD mouse following stimulation with control or *Rnls*^{mut} NIT-1 cells. Wells without NIT-1 cells or with PMA and ionomycin were used as negative and positive controls, respectively. Data are representative of three independent experiments. Data were compared by one-way ANOVA with Tukey's multiple comparison test. ns, not significant, *** *P*=0.0001. All data show mean ± SEM.
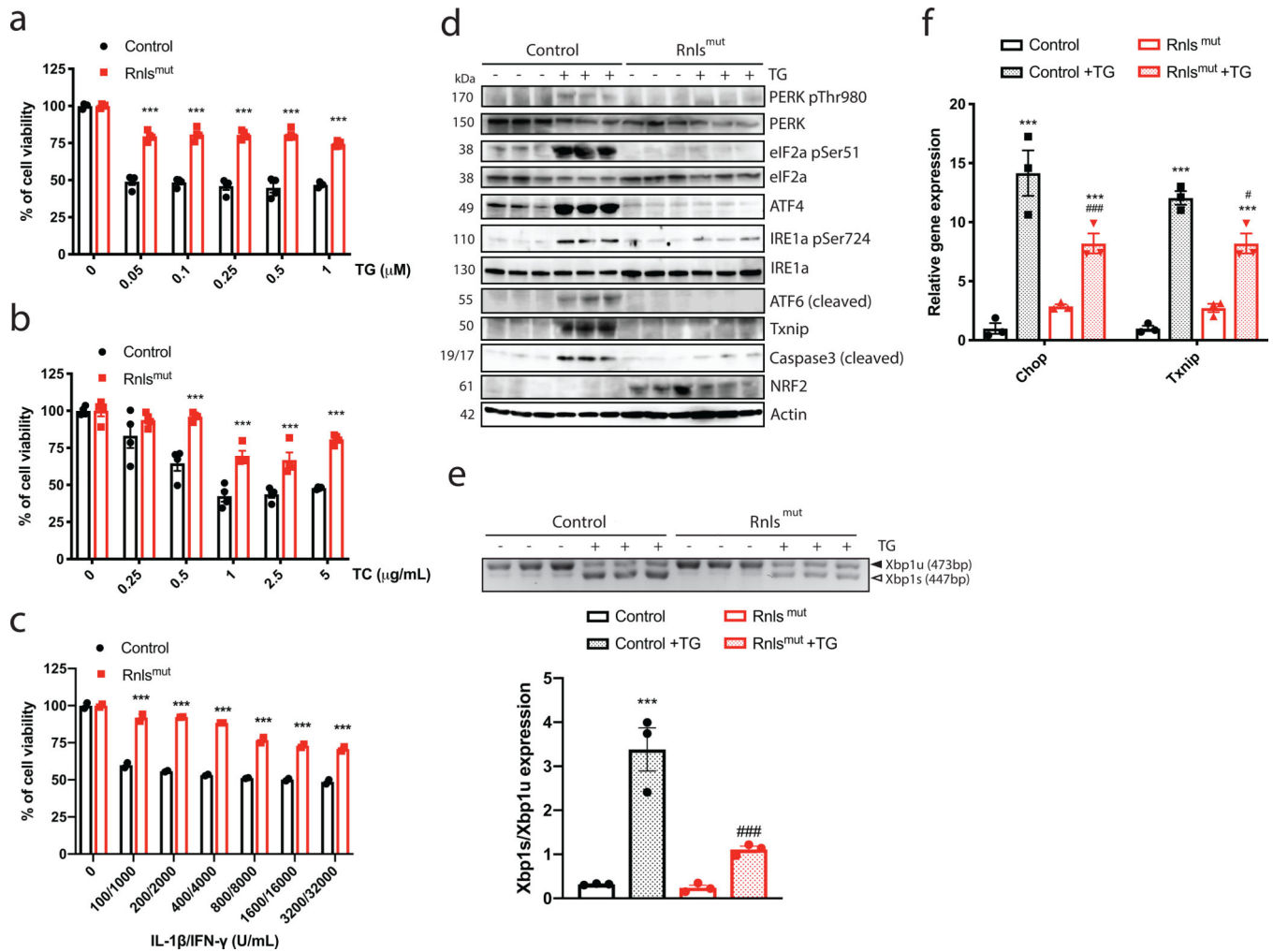
Fig. 4. *Rnls* deficiency confers ER stress resistance.

a,b: Cell viability measurement 24 h after thapsigargin (TG) (**a**), tunicamycin (TC) (**b**) and cytokine (IL-1β and IFN-γ)(**c**) treatment. Data show mean ± SEM of n=2–4 technical replicates per condition and are representative of 2–3 independent experiments. ****P*< 0.0001, calculated by two-way ANOVA with Sidak's multiple comparisons test. **d-f:** Measurement of the UPR in response to TG challenge. ER stress pathway protein phosphorylation (PERK, eIF2a and IRE1a), expression (ATF4, Txnip, NRF2) and cleavage (ATF6, Caspase3) (**d**), Xbp1 splicing (**e,** ****P*< 0.0001, [###]*P*=0.0005) and *Chop* and *Txnip* mRNA levels (**f,** ****P*< 0.0001, [#]*P*=0.0268, [###]*P*=0.0008) were measured in control and *Rnls*[mut] NIT-1 cells treated with or without 1 μM TG for 5 h. Data show mean ± SEM, n=3 per group and are representative of two independent experiments, calculated by one-way ANOVA with Dunnett's multiple comparisons test. * Control vs. Rnls[mut] cells in non-treatment group; # Control vs. Rnls[mut] cells in TG-treatment group (**d** and **e**).
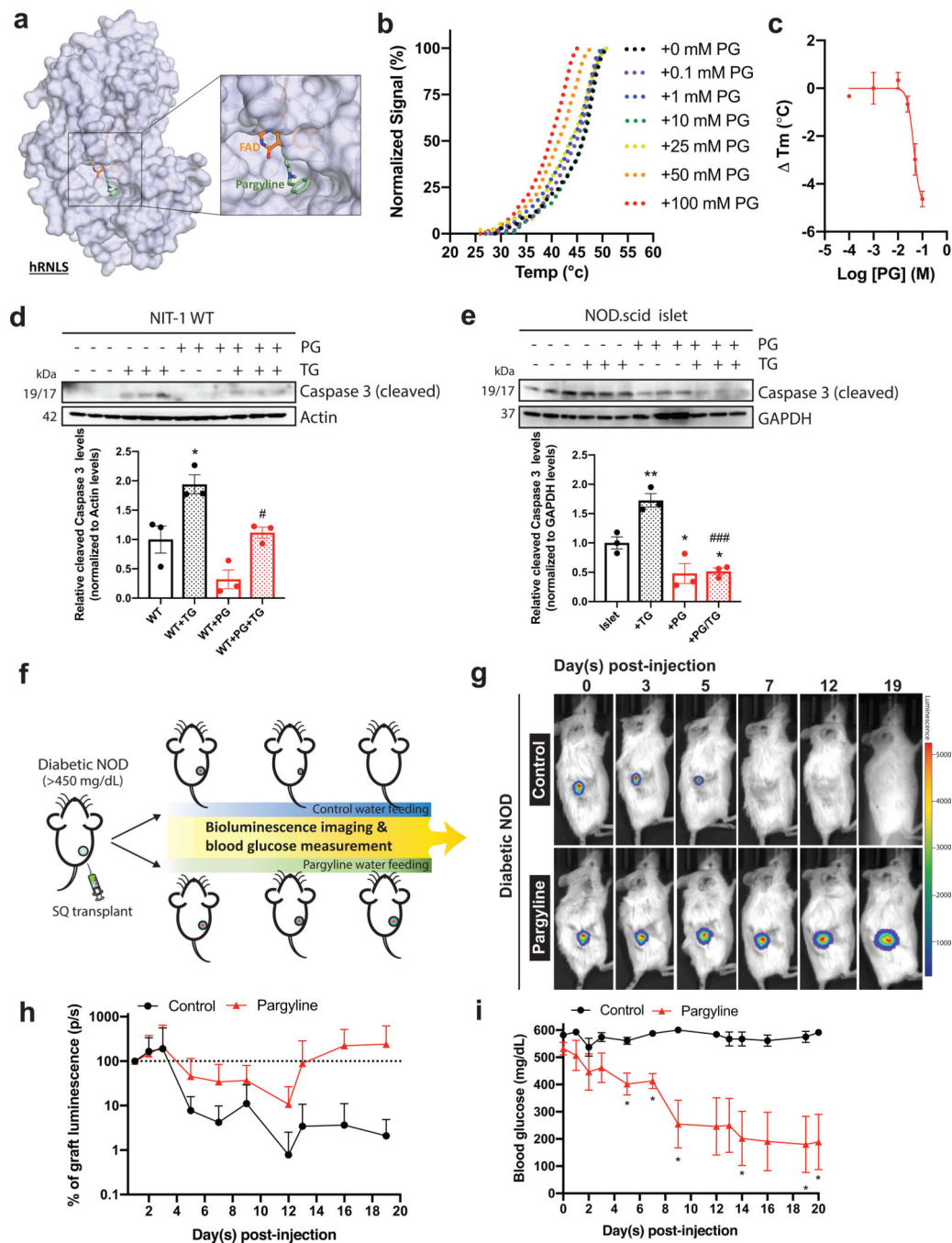
Fig. 5. The FDA-approved drug pargyline binds RNLS and protects beta cells against autoimmunity

a: Structural model of Pargyline in complex with human RNLS (hRNLS). The protein is shown in cartoon and surface representation. Pargyline (green) and co-factor FAD (orange) are shown as sticks. **b:** Human recombinant RNLS protein denaturation profile in the presence and absence of pargyline (PG) by a SYPRO orange protein-dye-based thermal shift assay. **c:** RNLS melting temperature (Tm) change in response to pargyline. Data were fit to a variable slope four-parameter sigmoid curve. n=3 technical replicates per condition,

representative of two independent experiments. **d,e:** Apoptotic response measured by caspase-3 activation in NIT-1 cells (**d**, *P= 0.0112, #P= 0.0223) and NOD.*scid* islet cells (**e**, *P= 0.0359 and 0.0495 for +PG and +PG/TG group respectively, **P= 0.0065, ###P= 0.0003) 5 hours after thapsigargin (TG) treatment in the presence or absence of PG. Data show mean ± SEM of n=3 per condition, calculated by one-way ANOVA with Dunnett's multiple comparisons test. * Comparison to WT or islet; # comparison to WT+TG or +TG. **f:** Experimental approach used to test pargyline for the protection of NIT-1 cells transplanted into diabetic NOD mice. **g:** Representative images of graft luminescence at days 0, 3, 5, 7, 12 and 19 post- transplantation. **h:** Proportion of remaining graft luminescence relative to day 0 (100%). **i:** Blood glucose levels in the control and pargyline treated mice over time, *P= 0.0316, 0.0053, 0.0367, 0.0422, 0.0381 and 0.0357 at days 5, 7, 9, 14, 19 and 20. Data show mean ± SEM of n=5 mice per group and are representative of three similar experiments, calculated by two-way ANOVA with Tukey's multiple comparisons test.
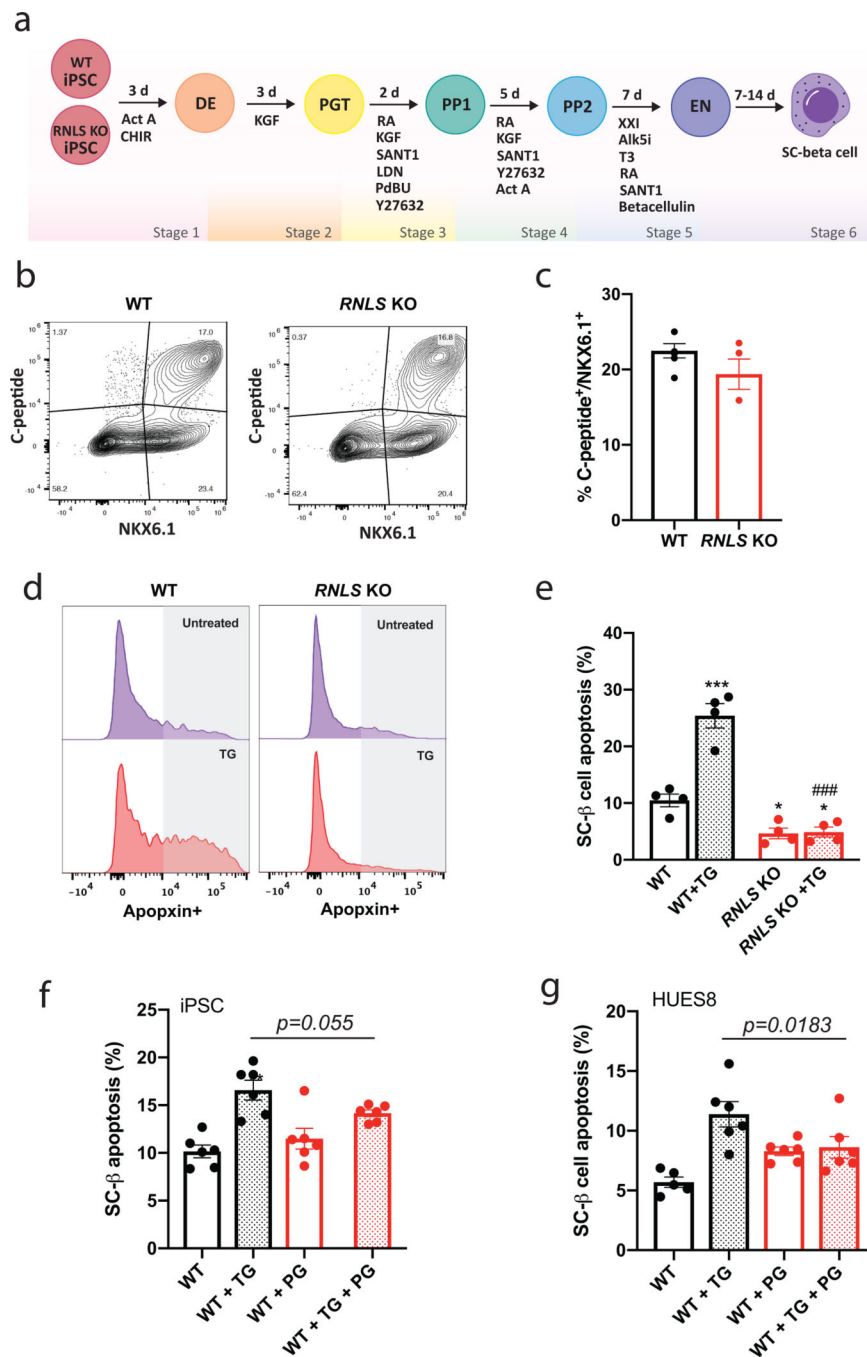
Fig. 6. *RNLS* deletion or inhibition protects human SC-beta cells against ER stress.
a: Schematic representation of the differentiation protocol used to generate SC-beta cells from isogenic wild-type (WT) and *RNLS* KO human iPSC. **b,c:** Representative flow cytometry analyses (**b**) and quantification (**c**) of the proportion of differentiated iPSC cells that co-expressed C-peptide and NKX6.1 as markers of beta cell identity. Data show mean ± SEM of n=6 (WT) and n=4 (RNLS KO). **d,e:** Representative flow cytometry analyses (**d**) and quantification (**e**, *P= 0.028 and 0.0348 for RNLS KO and RNLS KO+TG group respectively, ***$P < 0.0001$, ###$P < 0.0001$) of SC-beta cell death following TG treatment,

measured by the apoptosis dye apopxin within CD49a$^+$ beta cells[41]. Data show mean ± SEM of n=4 per condition and genotype. * Comparison to WT; # comparison to WT+TG. **f,g:** Apoptosis in CD49a$^+$ iPSC- (**f**) and embryonic stem cell- (HUES8) (**g**) derived beta cells challenged with TG in the presence or absence of pargyline (PG), n=6 per condition and genotype. Data show mean ± SEM, calculated by two-tailed unpaired t-test (**c**) and one-way ANOVA with Dunnett's multiple comparisons test (**e-g**).